

# NAVAL RESEARCH REVIEWS

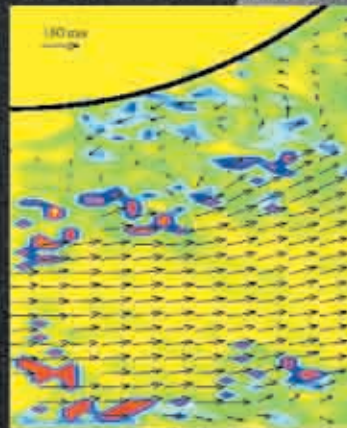
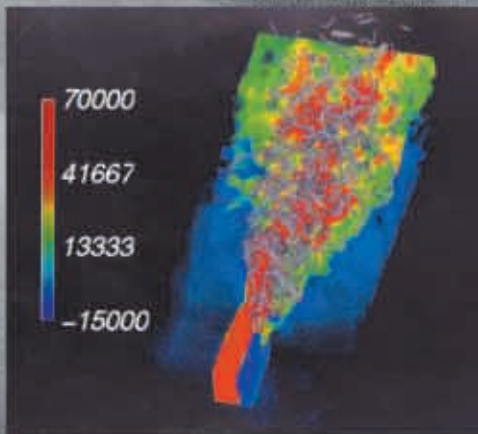
Volume 51, Number 3 & 4/1999

## Air Breathing Chemical Propulsion: Meeting the Challenges

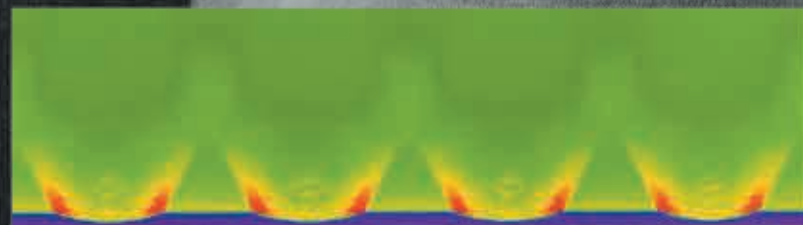
Timing is Everything p. 2

Laser Solved Mysteries p. 14

Going with the Coflow p. 24



and more ...



# From the Guest Editor . . .

Chemical propulsion had to meet several challenges over the past few decades due to changing requirements and constraints posed by the operational scenario. Improved range and speed from compact engines demand improved efficiency and performance in concert with reduced drag. Better operational maneuverability and reliability require combustion control both passively and actively over the entire flight range. The dawn of high speed computing and advanced diagnostics has opened up avenues in propulsion research hitherto considered impossible. These provide the capability of predicting performance and creating parametric characterization of propulsion systems, as well as making non-intrusive, *in-situ* measurements of the necessary species and other quantities.

The ONR propulsion program focuses on research to meet the above-mentioned challenges. In a nutshell, the program addresses research that generates the understanding and information required to develop propulsion systems for longer range, higher speed, better maneuverability, improved stealth, increased efficiency, minimized emission, enhanced reliability and reduced cost. The three possible scenarios of achieving this very complex goal are (i) improved mixing and control of precombustion, during combustion, and post-combustion processes, both actively and passively, (ii) utilization of fuels with higher energy density and better combustion characteristics and (iii) employment of thermodynamic cycles that are more efficient. Though all these three research scenarios are addressed in the ONR research program, the first aspect is emphasized in the articles included in this issue of Naval Research Reviews.

The significance of active control of combustion, and how it can be applied to reduce combustion-induced pressure oscillations and instability and to improve combustion performance, is elucidated in the article by Prof. Ken Yu of Naval Air Warfare Center-Weapons Division, China Lake. The research group in China Lake has pioneered the application of passive combustion control by the use of non axis-symmetric nozzles and inlets, and extended their work to active control with sequential fuel injection in gaseous fuel combustion. Prof. Yu is now applying this technology to liquid-fuel combustion, which is of primary interest to the Navy. The timing of fuel injection with respect to the vortices formed in the fuel/air mixture has a dramatic effect in reducing combustion pressure oscillations, reducing soot formation, and improving combustion efficiency. This has now become a topic of world-wide research.

In order to improve performance and to obtain other characteristics as described earlier, one has to physically measure the various combustion parameters and interpret the results as quickly as possible, preferably *in-situ*, so that the mechanisms involved could be understood, the numerical computer codes can be validated, and the predictive and design capability can be improved. To this end, ONR has invested in various diagnostic technique development, and acquisition of state-of-the-art instrumentation related to combustion. Prof. Ron Hanson from Stanford University, in his article, addresses the challenges and the approach he has taken to make combustion measurements with the temporal and spatial resolution required.

Post-combustion control involves control of plume characteristics, flame signature and emission, as well as plume trajectory. Research on control of the jet plume with counter current flow has resulted in the invention of a novel fluidic multi-axis thrust vector control. Here the exhaust jet itself, instead of mechanical fins, is performing the thrust vector function, thereby eliminating the drag induced by external mechanisms such as fins or bend-bodies. Prof. A. Krothapalli of Florida State University and Prof. Paul Strykowski of University of Minnesota address this development in their article.

The scientific information generated by the ONR basic research has been successfully applied in various propulsion component designs such as ducted rockets, partially premixed combustors, and stator-rotor designs. In his article, Dr. Hukam Mongia of General Electric Aircraft Engines elucidates the challenges in the design of future gas turbine engine combustion systems. The advances made in computational combustion dynamics are being utilized together with probability density function approaches. The formulation and validation of various models used in the code are described.

The ONR propulsion program is well coordinated with other sponsoring agencies and industry so that research findings can be transitioned into applications. A balanced analytical, computational, experimental approach is pursued. It is poised to offer excellent contributions in the fundamental and applied areas with innovative concepts, simulations, diagnostics, and experimentation.

**Gabriel D. Roy**  
*Office of Naval Research*





# NAVAL RESEARCH

## REVIEWS

### **2 Timing is Everything**

**A Study on Active Combustion Control  
for Advanced Combustors**

*by K. H. Yu and K. C. Schadow*

### **14 Laser Solved Mysteries**

**Diode-Laser Absorption Sensors for  
Combustion Measurements and Controls**

*by Ronald K. Hanson and Douglas S. Baer*

### **24 Going with the Coflow**

**Vectoring Thrust Using Confined Shear  
Layers**

*by P. J. Strykowski and A. Krothapalli*

### **35 Runway Models**

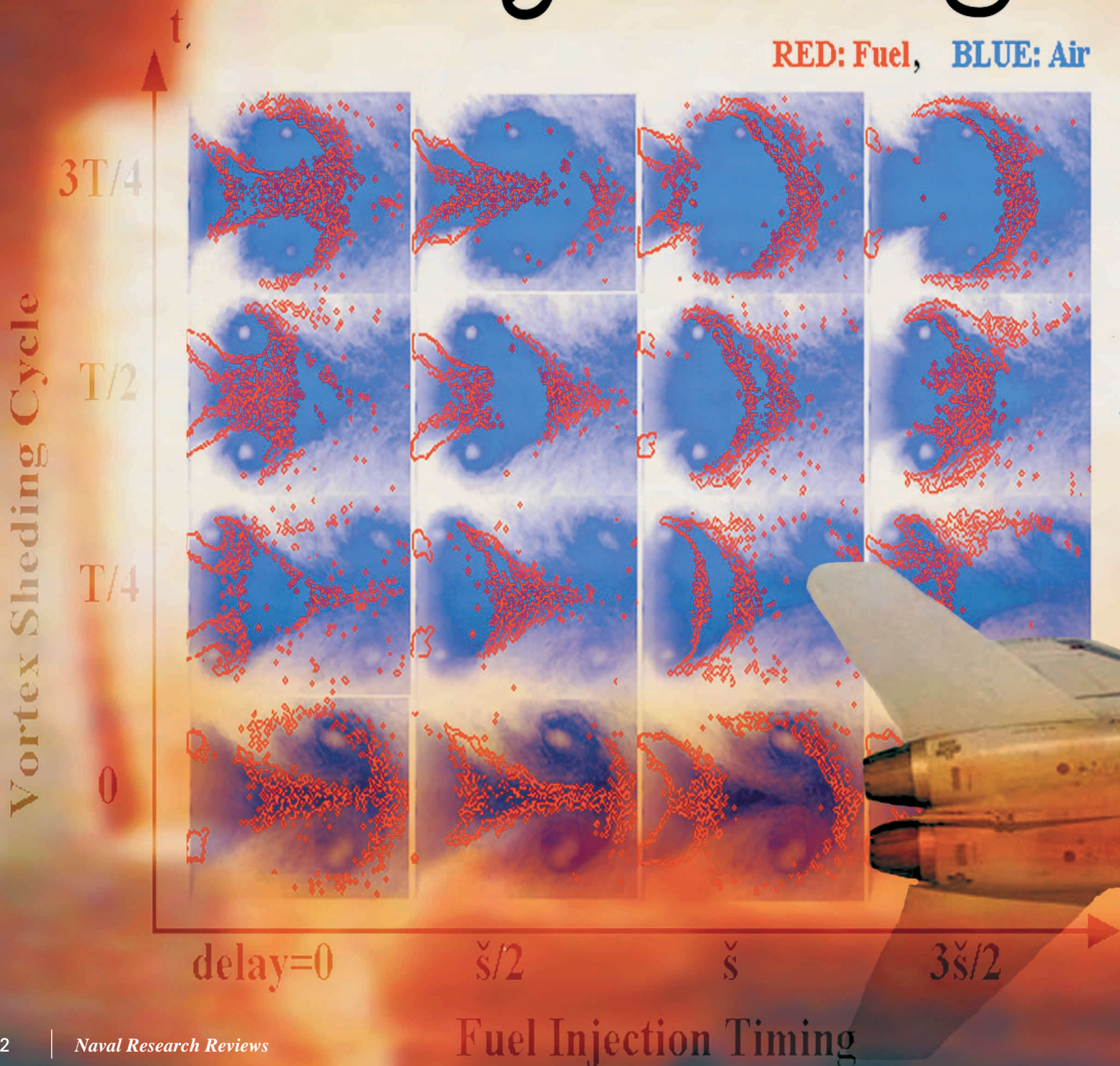
**Aero-Thermal Design Methodology for  
Gas Turbine Combustion Systems:  
Future Direction**

*by Hukam C. Mongia*


### **45 Profiles in Science**

*Dr. Ronald K. Hanson*

# Timing is Everything





A fighter jet, possibly an F-16, is shown in profile, flying towards the right. The aircraft is white with grey markings. The background is a dramatic, fiery orange and red, suggesting a sunset or a high-speed burn. The jet's wings are swept back, and it has several missiles mounted under the wings. The overall image has a high-contrast, almost abstract quality due to the color palette.

**T**he Navy wants to build a better combustor—a dump combustor to be more specific; the kind of passive intake, liquid-fueled device found on ramjet missiles and other military technology. In the past, scientists have improved performance by changing the shape of the combustor, a trial-and-error-method that is both expensive and time consuming. Researchers at the Naval Air Warfare Center, China Lake, believe the key lies in timing, not geometry.

In the following article, Yu and Schadow study the physical mechanisms and critical processes that affect combustion control, and experiment with fuel-injection and fuel-distribution techniques. They

were able to improve performance by actively controlling the injection of fuel directly into the combustor. The switch in emphasis from space-based to time-based control eliminates the need for costly design changes and makes it possible to construct new combustors from readymade components using an open-architecture system. Ultimately, these results may aid the researchers in developing a practical combustor control system for future propulsion systems. *- J.P.*

---

# A Study On Active Combustion Control For Advanced Combustors

---

**K. H. Yu\* and K. C. Schadow**

*Naval Air Warfare Center  
China Lake, CA*

---

## Abstract

Active combustion control (ACC) is an emerging art of regulating combustion performance using a dynamic hardware component that rapidly modifies combustion input. With the recent advances in electronics, it is becoming a very popular technology in propulsion and power industries. Yet, adapting such technology into practical combustors has proved difficult, due to lack of sufficient physical understanding. In this paper, we describe an experimental effort at the Naval Air Warfare Center to study basic mechanisms of ACC involving a dump combustor and present some of the results which will shed more light on various issues and processes of practical significance. The focus of our study was to provide scientific basis for implementing a fast-response *in-situ* closed-loop ACC system for liquid-fueled ramjet dump combustors. This technology employs an open-architecture-type design, and a successful transition of the results will revolutionize the way that combustion control is performed in advanced propulsion systems.

## 1. Introduction

As the requirements for future military combustors become increasingly demanding, an advanced combustion control system that can effectively shorten the combustor development time and improve the combustor performance will be an important technological asset to our military. Active combustion control (ACC) is an attractive idea because it relies on proper timing of fuel injection rather than spatial changes of flowfield as required in passive approaches. Since timing adjustment is simpler than the potential geometry modifications associated with passive control, ACC provides flexibility in performance and eliminates costly design changes.

In the past, studies on ACC have been motivated by undesirable combustor behaviors, that include combustion instabilities [1-10], poor burning efficiency [10-13], limited operational range [10,14], and excessive production of pollutants. [10,12,13,15] These studies have contributed greatly to the present understanding of fast-response ACC, but most of the previous ACC studies utilized gaseous fuel instead of more practical liquid fuel. Even in the studies that involve liquid fuel, fuel was either added upstream in a pre-vaporized state [6,9] or injected in a steady fashion [13], compromising the practicality of the ACC system and limiting the flexibility associated with temporal responsiveness.

Several technological challenges still remain before the ACC technique can be implemented to practical propulsion systems. One such challenge is to use liquid fuel for control and minimize the fuel amount by directly pulsing it into the combustion chamber. Because of the combustion delays associated with liquid-fuel atomization, droplet heating, vaporization and burning processes, it has been difficult to perform fast-response *in-situ* control using liquid fuel. Also, it was difficult to actuate liquid-fuel injection at high frequencies. As a result, such a control has not only been difficult to obtain, but the physical processes were also poorly understood.

The present study was motivated by our desire to extend ACC to liquid-fueled combustors and explore the use of ACC approach in practical propulsion systems. Recent progress in liquid-fuel actuator technology and enhanced understanding of the combustor dynamics provided an ideal background to further advance ACC technology to liquid-fueled processes. Thus, novel ACC experiments have been performed in a generic dump combustor using pulsed liquid fuel injection. The objectives are to establish closed-loop ACC using direct liquid-fuel injection, better understand the physical mechanisms as well as limitations, and provide the scientific basis

---

\* Presently Associate Professor, Aerospace Engineering Department, University of Maryland, College Park, MD.

for applying fast-response *in-situ* combustion control in practical propulsion systems. Ultimately, this will lead to the development of practical ACC technology for advanced liquid-fueled ramjets.

## 2. Theoretical Consideration

Understanding heat release dynamics is an important prerequisite for designing an efficient ACC system. Heat release process is critical not only for thermodynamic considerations but it is also important due to interactions with fluid dynamic and acoustic processes, that affect combustor performance. To enhance combustor performance actively requires an ability to modify the dynamics of heat release process both spatially and temporally. While actuators modulate fuel mass flux providing some means of temporal control, droplet interaction with flow features could be used to disperse fuel droplets affecting spatial heat release. Also, as will be shown in this section, fuel droplet size is an important factor which affects both timing and location of heat release.

### 2.1 Combustion-Acoustic Interaction (timing of heat release)

The interaction between pressure fluctuation and heat release fluctuation is an important consideration in ACC, because, depending on the relative phase lag between the fluctuations, the interaction may result in either a sourcing or a damping term for acoustic energy. According to well-known Rayleigh criterion [16,17], the change in acoustic energy density after one oscillation cycle can be written in terms of pressure oscillation,  $p'$ , and heat release oscillation,  $q'$ .

$$\Delta E \approx \int_V \Delta \varepsilon dV = \int_V \frac{\gamma-1}{\gamma} \int_t^{t+1/F} \frac{p' q'}{\bar{p}} dt dV \quad (1)$$

where higher order terms are neglected. Equation (1) can be derived from the governing equations of continuity, momentum, energy, and state by applying perturbation technique and linearizing the results.

According to Equation (1), if  $p'$  and  $q'$  are out of phase, then their product will be negative and the interaction results in acoustic energy loss, damping the oscillations. Therefore, one key strategy in active instability suppression is to actively create additional  $q'$  at out of phase with respect to  $p'$  so that the oscillation will be damped by acoustic energy loss. In general, since  $q'$  is very sensitive to the instantaneous fuel flux, a small amount of fuel flux can be modulated to achieve this task. The relative amplitude of properly phased  $q'$  necessary to suppress instability depends on how promptly the instability must be suppressed as well as the amplitude of instability  $p'$ . For instance, the acoustic energy contained in an oscillation cycle is

$$E = \int_V \varepsilon dV \quad \text{where}$$

$$\varepsilon = F \int_{1/F} \frac{\bar{p}}{2} \left( u'(t)^2 + \left( \frac{p'(t)}{\bar{p} c} \right)^2 \right) dt \quad (2)$$

whereas the maximum amount of suppression possible when  $p'$  and  $q'$  are perfectly sinusoidal and out of phase everywhere can be deduced from Equation (1) as

$$\Delta \varepsilon \approx - \frac{(\gamma-1)}{2 \gamma \bar{p} F} \frac{|p_{\max}'| |q_{\max}'|}{F} \quad (3)$$

To completely suppress the total amount of acoustic energy in Equation (2) after only one cycle, the amplitude of controlled heat release needs to be at least

$$|q'| \approx \frac{f}{2(\gamma-1)} \left[ \frac{(\bar{p} c |u_{\max}'|)^2}{|p_{\max}'|} + |p_{\max}'| \right] \quad (4)$$

Smaller  $q'$  will take more than one cycle to suppress the oscillations.

### 2.2 Flow Structure-Droplet Interaction (location of heat release)

In order to supply the fuel droplets into a desired location, one can point the injector to the location and directly inject the droplets. While this is intuitively straight forward, it will work only for large droplets that are relatively unaffected by fluid motion – those droplets that are unsuitable for combustion control. The better method for combustion application is to use the fluid motion and the interaction of fuel droplets with the fluid motion to guide the droplets.

The extent of the interaction between liquid fuel droplets and large-scale turbulent flow features such as vortices is expressed in terms of the particle Stokes number,  $Sto$ , which is the ratio of the characteristic time scale for particles responding to the fluid motion and that for the flow dynamics. The particle response time is estimated by assuming the drag on the particle (or fluid droplets [18]) follows Stokes's law ( $Re < 1$ ). For particle density  $\rho_f \gg \rho_g$ , the response time is taken to be

$$\tau_p = \frac{\rho_f D^2}{18 \mu_g} \quad (5)$$

which equals the time needed for the velocity difference to be reduced to  $e^{-1}$  of the original velocity difference. To assess the interaction with large vortices, the flow time scale



can be defined as the large eddy turn-over time or simply the period of vortex shedding. Then the resulting Stokes number can be written as

$$Sto = \frac{\rho_f D^2 F}{18 \mu_g} \quad (6)$$

and  $Sto$  determines the degree of interaction between the droplets and vortices.

The droplets with very small  $Sto$  follow fluid motion very closely with their physical location being determined entirely by fluid motion, while the droplets with very large  $Sto$  are nearly unaffected by fluid motion and follow ballistic trajectories. Recent experiments [19-21] and computations [22,23] suggested that only those droplets with  $Sto$  on the order of unity are affected by fluid motion and yet have enough momentum to be dispersed further outside the carrier fluid path. Because small droplets burn efficiently with short time delay, they are desirable for combustion control. For controlling spatial fuel distribution, those droplets with Stokes number close to unity would also be desirable, because they disperse even further outside via partial interaction with the structures yet sufficiently small for effective combustion. If droplet size distribution was such that those droplets with the latter characteristics constituted the upper end of the size distribution, more control over spatial distribution of fuel droplets could be obtained without compromising efficient combustion.

### 2.3 Effect of Fuel Droplet Size (factors affecting the heat release)

As shown in the previous section, it is important to control the timing and location of  $q'$  for instability suppression. While one can influence the relative phase of  $q'$  by controlling the timing of additional fuel flux, there is certain time lag between the fuel flux modulation and the resulting effect on heat release. For liquid-fueled control, the time lag is a sensitive function of the fuel type as well as the actuator and the flowfield characteristics. In particular, fuel-drop size distribution will have a significant impact because of the delays associated with droplet heating and vaporization processes.

In general, liquid fuel droplets will attenuate the effect of fuel flux modulation by delaying the mixing process and thus adversely affecting combustion response. A wide distribution of fuel droplet sizes will further attenuate the response. To assess the effect of droplet size, one may consider droplet heating and vaporization stages separately. As a first order approximation, one may assume that no vaporization takes place while the droplets are being heated and the heat flux into the droplets during this period is used to uniformly raise the droplet temperature. While these assumptions are not rigorous, they are nevertheless adequate approximations in

the present case where the vapor pressure is low and the Biot number for droplet heating is small.

Under these assumptions, the fuel temperature during the droplet heating period can be written as

$$T_f(t) = (T_f(0) - T_g) \exp\left[\frac{-6h}{\rho_f c_p D_0} t\right] + T_g \quad (7)$$

which is applicable until the droplet temperature reaches the boiling point of fuel. Then, the characteristic time scale associated with the induction period can be related to the fuel droplet size as

$$\tau_h \propto \frac{\rho_f c_p D_0}{6h} \quad (8)$$

Furthermore, the average heat transfer coefficient,  $h$ , which depends on the droplet Reynolds number,  $Re_f$ , would vary as  $D_0^{-0.4}$  [24] in the range of conditions likely to be encountered here. Therefore, the induction time associated with the droplet heating depends on the initial droplet size and would vary according to

$$\tau_h \sim D_0^{1.4} \quad (9)$$

which implies that the heat release process will not be synchronized unless the initial droplet size is uniform.

In this simple model, the droplet starts vaporizing when it is heated to the boiling temperature. For the vaporization process, one may further assume that all of the heat flux transferred into the droplet is used to vaporize the surface layer so that

$$h(\pi D^2)(T_g - T_f) \partial t^* = -\rho_f h_{fg} \partial V_f \quad (10)$$

which yields the rate of vaporization

$$-\frac{dV_f}{dt^*} = \frac{h\pi D^2(T_g - T_{fb})}{\rho_f h_{fg}} \quad (11)$$

Equation (11) has a maximum value when  $t^*=0$ . The heat release rate follows the rate of vaporization, provided that the mixing and combustion time delays are either much smaller or independent of the vaporization time scale. Then, the maximum amplitude of controlled heat release associated with single droplet burning is

$$Q_{\max} = \frac{\pi (T_g - T_{fb}) h h_{RP} D_0^2}{4 h_{fg}} \quad (12)$$



Since the number of droplets is inversely related to the volume of each droplet, the maximum magnitude of heat release oscillations for a given heat release potential is

$$(\Sigma Q)_{\max} = N_D Q_{\max} = \text{const} \cdot \frac{h(T_g - T_{fb})}{h_{fg} D_0} \sim \frac{\Delta T}{h_{fg}} D_0^{-1.4} \quad (13)$$

This implies that pulsed fuel sprays with smaller droplet size will be more effective in generating controlled heat flux oscillations.

### 3. Experiments on Active Instability Suppression

For active instability suppression, the approach we have taken is to pulse a small amount of liquid fuel at the instability frequency and adjust the timing using a closed-loop circuit. Figure 1a shows a schematic of a typical closed-loop ACC system applied to a ramjet dump combustor. The closed-loop ACC system consists of three separate components – sensor, controller, and actuator. The sensor is used to detect a change in combustion process, and the controller is used to make the proper actuation decision based on the

input from the sensor. The actuator then modifies the combustor input accordingly. The ACC system can be implemented in an open-architecture design by having each component in a modular form thus making an upgrade simple.

During unstable combustion process in dump combustors, large vortical structures are shed from the dump plane. [25] These vortices, that are typically formed at the instability frequency, play an important role in sustaining the oscillations. [25,26] The actuation may be best served by modifying such processes that affect the instability mechanism. In the present study, because our emphasis was on extending active control to liquid-fueled combustors, a simple phase-delay circuit was utilized instead of a more sophisticated controller using adaptive technique. Figure 1b shows the actual configuration which was used to actively regulate the fuel injection scheduling at the dump plane. A pressure transducer was used as a sensor. In the controller, the pressure transducer signal was filtered and phase-shifted to produce square wave that regulated the fuel flux through the actuators. Two sets of actuators with different atomization characteristics were used in the experiment.

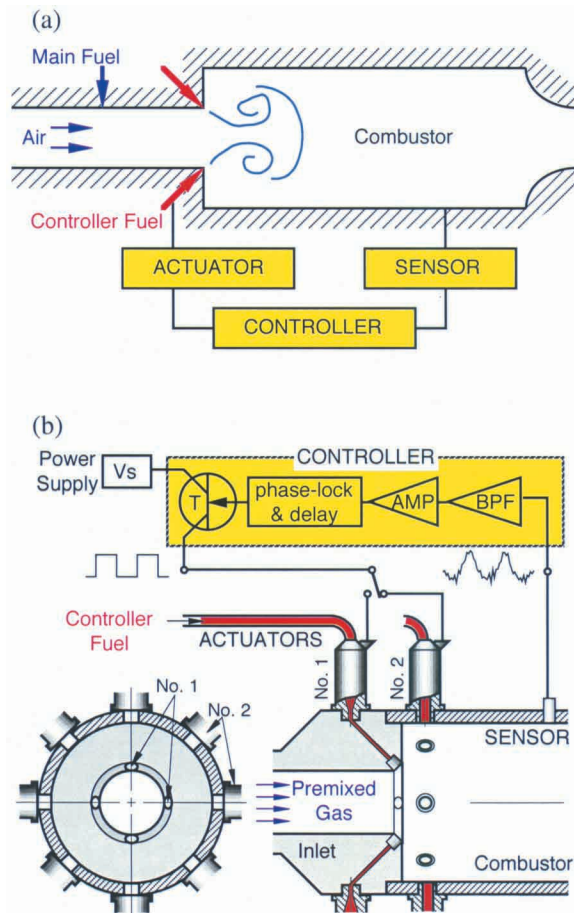


Fig. 1 – Schematics of the closed-loop control system applied to the dump combustor.

Table 1 – Dump combustor setup for the corresponding cases.

The diagram shows a cross-section of the dump combustor. It has an 'inlet' on the left, followed by 'liquid fuel actuators' (No. 1 and No. 2). The combustor length is labeled 'Lcomb' and the diameter is 'dcomb = 2.46'. At the right end, there is a 'nozzle' with diameter 'dnozz' and length 'Lnozz'. The inlet length is 'Linlet'. The diagram also shows 'Ethylene' and 'air' entering the inlet. The overall length of the combustor section is 'Lcomb'.

Case	Liquid Fuel	actuator	$L_{inlet}$	$L_{comb}$	$d_{nozz}$	$L_{nozz}$
1	Ethanol	No. 1	58.5	10.2	1.29	1.85
2	Heptane	No. 1	25.8	12.4	0.615	1.85
3	Heptane	No. 1	25.8	12.9	0.862	1.32
4	Heptane	No. 1	25.8	8.9	0.615	1.85
5	JP-10	No. 2	20.2	15.4	1.36	1.81

all dimensions are in terms of  $d_{inlet} = 42$  mm

Table 1 shows the dimensions as well as the configuration of the model ramjet dump combustor, in which the ACC experiments were performed. Air was supplied from high-pressure storage tanks and was metered using a choked orifice nozzle which also defined the upstream acoustic boundary of the inlet. Fuel was injected both in a steady fashion and in a temporally controlled way at the dump plane. A long-radius type exhaust nozzle was used at the downstream end of the combustor. In an actual system, the actuator fuel would be only a small fraction of the total fuel. For the steady portion of the fuel flux, ethylene was supplied

**Table 2 – Average flow conditions and characteristic parameters for test cases.**

Operating Conditions				Instability		Control	
Case	Power Output (kW)	Re	$\phi$	$\frac{p'_{rms}}{\bar{p}_{comb}}$	F (Hz)	% fuel pulsed	D <sub>32</sub> (μm)
1A	66	7.7 10 <sup>4</sup>	0.47	0.008	34	30	50
1B	82	7.7 10 <sup>4</sup>	0.58	0.005	35	25	50
2	180	2.0 10 <sup>5</sup>	0.51	0.042	87	15	39
3A	270	2.5 10 <sup>5</sup>	0.59	0.092	98	12	36
3B	360	3.4 10 <sup>5</sup>	0.57	0.089	96	8.0	38
4	180	2.0 10 <sup>5</sup>	0.51	0.054	95	15	39
5A	630	4.4 10 <sup>5</sup>	0.72	0.076	120	15	10
5B	580	4.4 10 <sup>5</sup>	0.69	0.11	120	7.9	10
5C	560	4.4 10 <sup>5</sup>	0.66	0.095	122	4.1	10
5D	1280	1.0 10 <sup>6</sup>	0.66	0.13	125	7.2	10
5E	1230	1.0 10 <sup>6</sup>	0.63	0.21	125	3.7	10
5F	1210	1.0 10 <sup>6</sup>	0.62	0.18	125	1.9	10

at a constant rate into the inlet duct. For the controlled flux, ethanol, heptane, or JP-10, which amounted to about 2 to 30 percent of the total fuel flux, was injected through the actuators. Instabilities were observed under certain conditions and a closed-loop fuel injection process was used to suppress the instabilities. Table 2 shows the specific operating conditions at which the unstable conditions were encountered. Some characteristic flow parameters are also shown for reference.

### 3.1 Establishing Control Authority With Liquid Fuel

In the present experiment, a novel approach which relied on timing-dependent fuel-droplet dispersion behavior was utilized. As explained previously, large vortical structures are shed during the unstable operation. The controller fuel was injected directly into these vortices at different timing with respect to their shedding process. Thus, the amount of slip velocity the droplets were subjected to was dependent on the injection timing. As a result, the droplet dispersion behavior was affected by the relative phase between the fuel injection and vortex shedding. Figure 2 shows the fuel droplet dispersion behavior with respect to the large vortex at various fuel injection timings. The red contour lines represent the phase-averaged Mie-scattering intensity data from fuel droplets, which are shown superimposed with the underlying vortex structures in blue. The droplets clustered in the core of the jet flow when fuel was injected after the vortex

shedding, while those fuel droplets injected ahead of the vortex shedding were subjected to the vigorous interaction and dispersed well into the recirculation zone.

A detailed ACC experiment was performed under Case 1 conditions. Based on average fuel flux, the thermal power output was between 66 and 82 kW. The instability in this case was related to the acoustic quarter-wave mode of the inlet. [27] When the timing of the liquid fuel injection was closed-loop controlled, the amplitude of pressure oscillations was very responsive to the controller parameter. Figure 3 shows the change in average spectral amplitude at the instability frequency as a function of the electronic-control-unit (ECU) phase delay. Under an improper phase setting, 20 degrees for instance, the oscillation amplitude remained high. The maximum amplitude in this case was close to the natural oscillation amplitude, that was obtained without closed-loop control. At the phase setting of 110 degrees, which corresponded to pulsed fuel injection synchronized with the vortex shedding process, the suppression of oscillation amplitude was most effective. Sound pressure level reduction of up to 15 dB was achieved using this method. When the flow conditions were changed slightly in Case 1B, the dependency on the injection phase remained unchanged from Case 1A.

Figure 4a shows the onset of active instability suppression, as the fuel injection timing was switched from the ECU setting of 20 degrees to 110 degrees at time  $t=0$ . With the timing change, the oscillation amplitude was quickly brought under control to about one-fifth of the uncontrolled level only after a few cycles. The injection frequency was unaffected by the injection timing change. Figure 4b shows a comparison of pressure spectra between a closed-loop injection case with the properly controlled injection timing and the baseline case without closed-loop control. The spectral amplitude was reduced significantly at all of the higher harmonic frequencies as well as at the fundamental. The results clearly

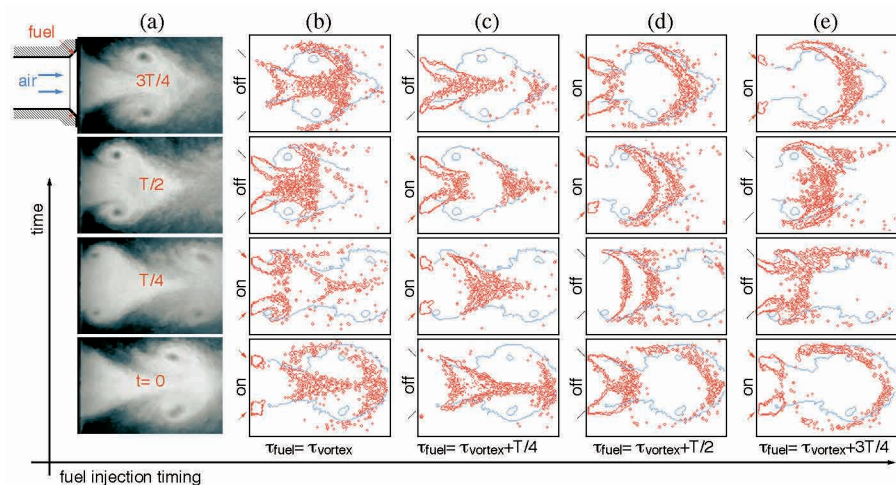


**Fig. 2 – Mie-scattering images of the flowfield showing vortex-droplet interaction as a function of the fuel injection timing.**



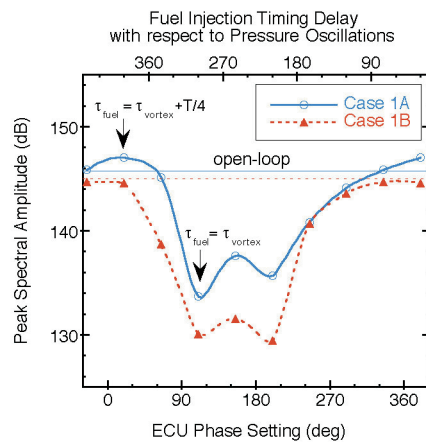


Fig. 3 – Pressure oscillation amplitude as a function of fuel injection timing.

demonstrates the potential of active instability suppression technique that is based on properly-timed pulsed fuel injection directly into the vortices.

### 3.2 Determining the Minimum Fuel Flux Needed

To explore more practical issues that would affect the transition of the above results, similar experiments were extended to higher flow conditions using the same actuators. However, instead of ethanol, liquid heptane was used as the controller fuel as heptane is about 66 percent more energetic per volume than ethanol. Furthermore, in this set of experiments, the combustor dimensions were varied as well as the flow conditions to find naturally unstable conditions at which ACC experiments could be performed. In general, the controller fuel flow rate (heptane) was held constant while the main air and main fuel (ethylene) flow rates were systematically increased. As a result, the controller fuel flux constituted increasingly smaller portion of the total fuel flux. The controller performance became marginal at 360 kW

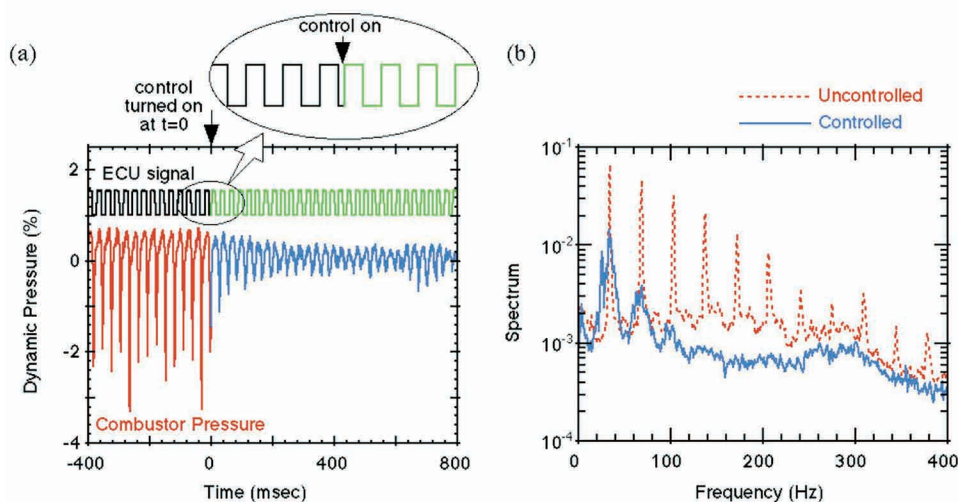


Fig. 4 – Comparison of controlled and uncontrolled oscillations. (a) Onset of active instability suppression, (b) Comparison of combustor pressure spectra.

output operation, suggesting a critical fuel flux was reached for maintaining the control authority.

In Figure 5a, the amount of relative reduction in peak spectral amplitude was plotted as a function of the inlet flow Reynolds number. Most of the data followed a general trend that indicated the diminishing control effectiveness with flow scale. However, this behavior was very gradual and was more related to the fact that the general amplitude of instability was greater at higher output conditions. On the other hand, there was a sharp increase in the number of cycles needed to reach the minimum amplitude at the on-set of ACC. Figure 5b shows the number of cycles it took to reach the controlled state as a function of the relative heat release potential of the controller fuel to the overall fuel. The results indicate that the control authority was marginal when the controller fuel flux was dropped to 8 percent of the total fuel flux. Using controller fuel flux below 8 percent, active instability suppression was unsuccessful in the present case.

## 4. Scaling Experiments With Different Actuators

Further scale-up tests were continued with different actuators (No. 2) and with JP-10 fuel, which was considered the likely fuel that would be used in practical systems. The No. 2 actuators were prototype fuel injectors that used air-assisted mechanism to obtain much finer sprays than the previous actuators. Air-assisted atomization required a small amount of secondary air flow, which was less than one percent of the air needed for stoichiometry. Figure 6 shows the transfer functions comparing the combustor response using No. 1 and No. 2 actuators. For the conditions at which the actuators were operated, the Sauter-mean diameter,  $D_{32}$ , was about four times smaller with No. 2 actuators than with No. 1 actuators.

This significant change in actuator characteristics also made it possible to study the effect of fuel droplet size on control efficiency.

### 4.1 Critical Fuel Flux

In the scaling experiments, up to eight actuators were employed at a time. By increasing the combustor thermal output while systematically reducing the number of actuators, the minimum controller fuel flux was again investigated experimentally. The results showed that the minimum fuel flux was dependent on the actuator characteristics. Using No. 2 actuators, the minimum fuel flux

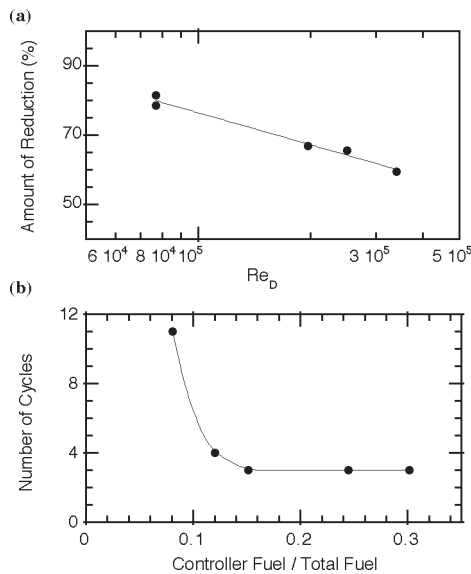


**Fig. 5 – Control effectiveness during scale-up experiments. (a) peak amplitude reduction .vs. inlet flow Reynolds number, and (b) required number of cycles to reach the controlled state .vs. pulsed fuel ratio.**

was found to be slightly below 2 percent of the total fuel flux. This can be compared with the limit with No. 1 actuators, which was about 8 percent. Figure 7 shows the plot of relative amount of controller fuel flux with respect to the relative amount of oscillation amplitude in the controlled cases. While there was slight decline in control effectiveness with decreasing amount of controller fuel flux, the controller became no longer effective below these limits.

Experimentally obtained values of the critical fuel flux was substantially different in the two sets of the scaling experiments. While there are many possible reasons for this behavior, the most significant effect will be due to the actuator and the fuel characteristics. Also, the effect of scale would have played a significant role. Figure 8 shows the

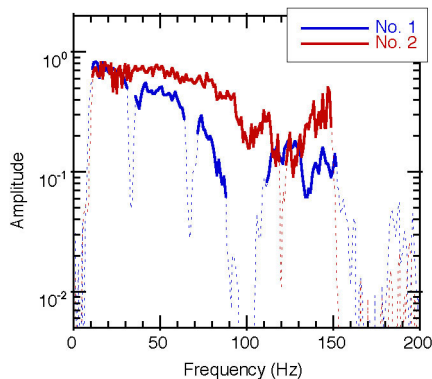


**Fig. 6 – Amplitude of transfer function between the combustor pressure oscillations and the driving signal using No. 1 injectors with Case 1 condition and No. 2 injectors with Case 2 condition.**

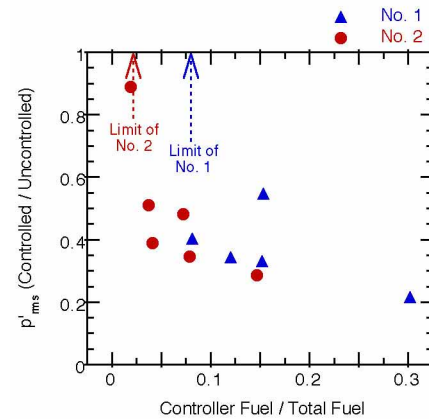


**Fig. 7 – Suppression of instability amplitude as a function of the relative amount of controller fuel.**

normalized magnitude of rms pressure oscillations as a function of the combustor thermal output. In general, the instability became much more severe at higher output conditions. This could be related to the fact that the amplitude of heat release oscillations per given volume increased with the scale-up process, as the higher output conditions were achieved by increasing the volumetric heat release rate.

#### 4.2 Effect of Fuel Droplet Size

During the scaling experiments, since the amplitude of instabilities was different in each case, it follows that the amount of fuel flux needed for control should also be different. To eliminate the effect due to the scale, each case was normalized by the magnitude of naturally occurring instabilities. Thus, using Equation (4), theoretical amount of controlled heat flux that was needed to suppress the given amplitude of instability was calculated, and this value was used in normalizing the controller fuel flux. Figure 9 shows the normalized relationship between heat flux and fuel flux. The heat flux was normalized by the theoretical amount of required heat flux considering the uncontrolled instability amplitude, while the fuel flux was taken as a simple ratio with the total fuel. The results showed a good overlap between the various cases that used three different fuels and two actuators.

It can be inferred from Figure 9 that actuator No. 2 was more effective than actuator No. 1 in suppressing the instabilities. Since No. 2 actuators produced much smaller drop size than No. 1 actuators, this trend was consistent with the expectation. The control process using No.1 actuators was not very efficient. The actual amount of fuel needed was more than 2.4 times that amount which is theoretically sufficient for suppressing the instability in just one cycle. However, with No. 2 actuators, the minimum fuel amount needed for control authority can be as low as 0.31 times the theoretical amount. As expected, many more cycles than one were required to suppress the instability as the controller fuel flux was relatively low.



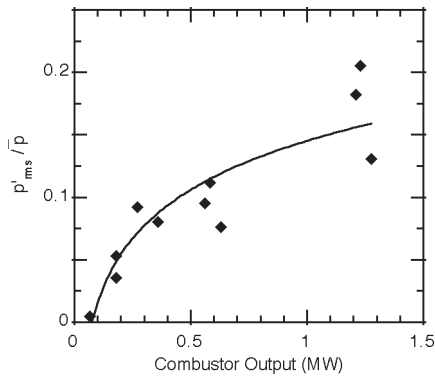


Fig. 8 – Observed instability amplitude at various scale-up conditions.

The actual amount of improvement in going from No. 1 to No. 2 actuators was about 7.7 fold reduction in the critical fuel flux. This can be compared with the expected dependency on drop size, which was discussed in section 2. From Equation (13), one would expect the improvement in heat release due to fuel drop size and fuel type to be

$$\left( \frac{\Delta T / h_{fg}}{\Delta T / h_{fg}} \right)_{JP-10} \times \left( \frac{D_{0, No.2}}{D_{0, No.1}} \right)^{-1.4} \approx 7$$

Considering that the analysis was for a simplified model case, the quantitative agreement in the present experiments is very good. Needless to say, such information can be used to estimate the critical fuel flux required for maintaining control authority in new combustors.

### 4.3 Limitation of Simple Phase-Delay Controller

The closed-loop approach using simple phase-delay was very effective in controlling instability when the oscillation frequency remained constant. However, for other cases, in which the instability frequency drifted with the onset of

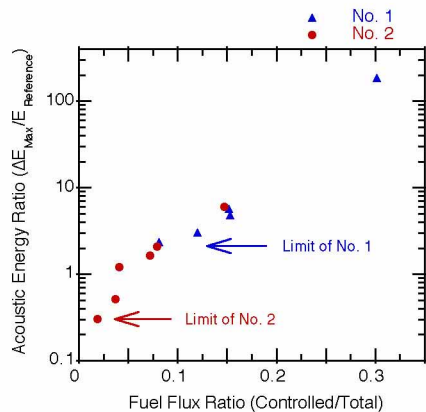


Fig. 9 – Theoretical ratio showing the potential amount of controlled heat release oscillations normalized by the acoustic energy of the instability.

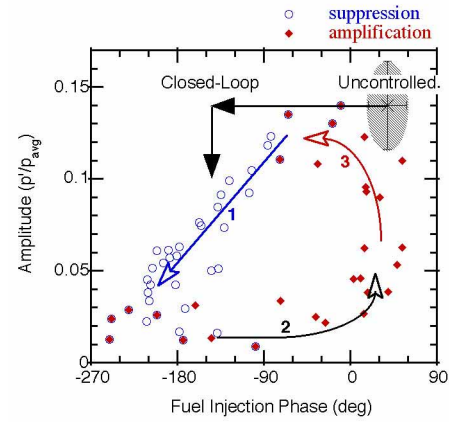


Fig. 10 – Observed ECU phase with respect to the oscillation amplitude of each cycle.

closed-loop fuel injection, this approach was not very practical because the oscillation amplitude periodically returned to the uncontrolled level after initial suppression. The main cause of this undesirable behavior was found to be frequency-dependent phase-shift, which is imposed by the band-pass filter in the simple controller.

Figure 10 shows a mapping of instantaneous amplitude and fuel injection phase in a typical case with the simple closed-loop control established. The shaded region represents the baseline behavior when the fuel injection was not closed-loop controlled. First, when the closed-loop control circuit was turned on, the fuel injection caused the heat release at the proper phase so that the oscillation amplitude started to be suppressed (process 1 in the figure). Then, as the amplitude was lowered, the instability frequency started to drift causing shift in the injection phase (process 2). Finally, if the injection phase shift became large enough, the heat release started occurring at the driving phase increasing the amplitude back to the original level (process 3). Then, the suppression processes repeated again as large-amplitude oscillations returned to the original frequency.

Such undesirable behavior may be avoided by employing a higher order control algorithm based on adaptive strategy or by adding other simple measures to ensure that the frequency remains constant. In adaptive control strategy, a secondary control loop can be employed that monitors the change in frequency and shift the phase settings accordingly. Also, in an alternative strategy, it may be possible to combine an open-loop injection at a constant frequency, that will prevent shift in the oscillation frequency. These ideas are being investigated in on-going experiments to demonstrate more robust control strategy suitable for practical systems.

## 5. Concluding Remarks

The opportunity exists to advance ramjet technology by incorporating our understanding of two-phase turbulent reacting flow in dump combustors with fast-response active

combustion control (ACC), which will replace current controls that are based on passive strategies. Typically, passive techniques for combustion control are limited in operability range and expensive to develop, since they require individually tailored spatial modifications of the flowfield and material. In contrast, active control techniques are based on precise scheduling of temporal events, thus minimizing unnecessary geometry changes. This switch in emphasis from spatial to temporal precision will allow more flexibility into the combustor design and will make it possible to implement open-architecture-type system design, which in the long run will revolutionize combustion control process.

Several milestones resulted from the present investigation. The first was to identify vortex-droplet interaction as a key process in controlling temporal as well as spatial distribution of controller fuel. Fuel distribution affects the heat release dynamics which is of critical importance in combustion control. Second, fast-response *in-situ*-type ACC was demonstrated using pulsed liquid-fuel injection directly into combustor vortices. Direct injection of fuel into the combustor is not only a practical design, but it also can be used to minimize the amount of controller fuel needed. Third, in scaling experiments, it was revealed that the amount of relative fuel flux played an important role in maintaining control authority. In the ensuing experiments, the critical amount of relative fuel flux was quantified as a function of the actuator and instability characteristics. Lastly, the dependence on fuel droplet size was derived and compared with the experimental data from the scale-up experiments. These results could be useful in developing more practical ACC technology for liquid-fueled dump combustors.

The present study was conducted not just to better understand the physical mechanisms and critical processes that affect the combustion control, but we were also motivated by our desire to develop ACC technology that will be practical for air-breathing propulsion systems. Thus, our earlier emphasis was on extending ACC to liquid-fueled combustors using a simple control strategy. Upon identifying the important physical mechanisms, we were able to inject liquid fuel directly into the dump combustor, and optimize the combustor performance by modifying the fuel injection timing that affected transient heat release. Detailed measurements were made to understand and explore various physical mechanisms and scaling issues, that may affect potential implementation of the research results. Presently, the investigation is continuing with an effort to explore other performance benefits of ACC and to make the control more robust and practical. It is our belief that such detailed mechanistic understanding combined with practical research goals will produce much needed scientific basis for properly designing and implementing ACC technology into future propulsion systems.

## Acknowledgment

This study was sponsored by the Office of Naval Research, with Dr. Gabriel D. Roy as the scientific officer.

## Biographies

**Ken H. Yu** received his B.S., M.S., and Ph.D. degrees in Mechanical Engineering from the University of California at Berkeley, in 1985, 1988, and 1989 respectively. He worked at NASA-Ames Research Center in 1985 as an aerospace engineer. He was a postdoctoral fellow/visiting professor at Ecole Central Paris, France, in 1989-1990. From 1990 to 1999, he worked as a physical scientist at the Propulsion Research Lab, Naval Air Warfare Center, China Lake, CA. He is currently an Associate Professor in the Department of Aerospace Engineering at the University of Maryland, College Park. His research interests are in the broad field of fluid dynamics, combustion, and optical and laser diagnostics. His research has resulted in more than 100 scientific publications in these subjects as well as 4 patents, some of which are still pending. His research has been acknowledged by three conference best paper awards from AIAA and JANNAF.

**Klaus C. Schadow** is presently a Senior Scientist at the Naval Air Warfare Center Weapons Division (NAWCWD) after serving as Head, Propulsion Research Branch, from 1977 to 1998. He received his Ph.D. in Mechanical Engineering in 1975 from the Technical University Munich, Germany. Dr. Schadow has been involved in a number of programs on passive and active mixing/combustion control with application to airbreathing missile propulsion, plume signature control, and compact incineration. Dr. Schadow has authored/co-authored over 300 publications, which include over 55 refereed journal publications and 12 patents.

## Nomenclature

$c$	= speed of sound
$c_p$	= specific heat at constant pressure
$D$	= fuel droplet diameter
$D_{32}$	= Sauter mean diameter of fuel droplets
$D_0$	= initial diameter of fuel droplet
$E$	= average acoustic energy in a cycle
$F$	= frequency of instability
$h$	= average heat transfer coefficient
$h_{fg}$	= latent heat of vaporization
$h_{RP}$	= enthalpy of combustion
$N_D$	= number of fuel droplets with size $D$
$\bar{p}$	= average pressure
$p'$	= fluctuating pressure
$q'$	= fluctuating heat release
$Q$	= rate of heat release from burning fuel droplet
Re	= Reynolds number
$t, t^*$	= time
$T$	= temperature
$u'$	= fluctuating velocity



$V$	= combustor volume
$V_f$	= fuel droplet volume
$\Delta E$	= change in acoustic energy after one cycle
$\Delta \varepsilon$	= change in acoustic energy density
$\varepsilon$	= instantaneous acoustic energy density
$\phi$	= equivalence ratio
$\gamma$	= ratio of specific heats
$\mu$	= dynamic viscosity
$\bar{\rho}$	= average density of combustor gas
$\rho_f$	= fuel droplet density
$\tau_h$	= characteristic heating time
$\tau_v$	= characteristic vaporization time

#### Subscripts:

avg	= average quantity
f	= characteristics of fluid drop
g	= characteristics of gas
max	= maximum quantity
n	= related to n-th cycle
rms	= root-mean-squared quantity

## References

- Candel, S.M., "Combustion Instabilities Coupled by Pressure Waves and Their Active Control," *Twenty-Fourth Sympo. (Inter.) on Comb.*, The Combustion Institute, Pittsburgh, PA, 1992, pp 1277-1296.
- McManus, K.R., Poinot, T., and Candel, S., "A Review of Active Control of Combustion Instabilities," *Prog. in Energy & Comb. Sci.*, 19:1-29 (1993).
- Lang, W., Poinot, T., and Candel, S., "Active Control of Combustion Instability," *Comb. & Flame*, 70:281-289 (1987).
- Bloxside, G.J., Dowling, A.P., Hooper, N., and Langhorne, P.J., "Active Control of Reheat Buzz," *AIAA J.*, 26:783-790 (1988).
- Poinot, T., Bourienne, F., Candel, S., and Esposito, E., "Suppression of Combustion Instabilities by Active Control," *J. Propul. & Power*, 5:14-20 (1989).
- Langhorne, P.J., Dowling, A.P., and Hooper, N., "A Practical Active Control System for Combustion Oscillations," *J. Propul. & Power*, 6:324-333 (1990).
- Schadow, K.C., Gutmark, E., and Wilson, K.J., "Active Combustion Control in a Coaxial Dump Combustor," *Comb. Sci. & Tech.*, 81:285-300 (1992).
- Gulati, A. and Mani, R., "Active Control of Unsteady Combustion-Induced Oscillations," *J. Propul. & Power*, 8(5):1109-1115 (1992).
- Sivasegaram, S., Tsai, R-F., and Whitelaw, J.H., "Control of Combustion Oscillations by Forced Oscillation of Part of the Fuel Supply," *Comb. Sci. and Tech.*, 105:67 (1995).
- McManus, K.R., Vandsburger, U., and Bowman, "Combustor Performance Enhancement Through Direct Shear Layer Excitation," *C.T., Comb. & Flame*, 82:75-92 (1990).
- Yu, K., Trouve, A., and Candel, S., "Combustion Enhancement of a Premixed Flame by Acoustic Forcing with Emphasis on Role of Large-Scale Structures," 29th Aerospace Sciences Meeting, AIAA-91-0367, 1991.
- Gutmark, E., Parr, T.P., Hanson-Parr, D.M., and Schadow, K.C., "Use of Chemiluminescence and Neural Networks in Active Combustion Control," *Twenty-Third Sympo. (Inter.) on Comb.*, The Combustion Institute, Pittsburgh, PA, 1990, pp 1101-1106.
- Brouwer, J., Ault, B.A., Bobrow, J.E., and Samuelsen, G.S., "Active Control for Gas Turbine Combustors," *Twenty-Third Symp. (Inter.) on Comb.*, The Combustion Institute, Pittsburgh, PA, 1990, pp 1087-1092.
- Gutmark, E., Parr, T.P., Hanson-Parr, D.M., and Schadow, K.C., "Closed-Loop Amplitude Modulation Control of Reacting Premixed Turbulent Jet," *AIAA J.*, 29 (12), 2155-2162, 1991.
- Parr, T.P., Gutmark, E.J., Wilson, K.J., Yu, K., Smith, R.A., Hanson-Parr, D.M., and Schadow, K.C., "Compact Incinerator Afterburner Concept Based on Vortex Combustion," *Twenty-Sixth Sympo. (Inter.) on Combustion*, The Combustion Institute, Pittsburgh, PA, 1996.
- Lord Rayleigh, *The Theory of Sound*, Dover, p.227, 1945.
- Putnam, A., *Combustion Driven Oscillations in Industry*, Elsevier, New York, 1971.
- Batchelor, G.K., *An Intro. to Fluid Mechanics*, Cambridge Univ. Press, 1967, pp.230-238.
- Lazaro, B.J. and Lasheras, J.C., "Particle dispersion in a turbulent, plane, free shear layer," *Phys. Fluids A* 1: 1035-1044 (1989).
- Longmire, E.K. and Eaton, J.K., "Structure and control of a particle-laden round jet," *JFM* 236: 217-257 (1992).
- Glawe, D.D. and Samimy, M., "Dispersion of Solid Particles in Compressible Mixing Layers," *JPP* 9 (1): 83-89 (1993).
- Chung, J.N. and Troutt, T.R., "Simulation of particle dispersion in an axisymmetric jet," *JFM* 186: 199-222 (1988).
- Chang, E. and Kaliasanath, K., "Simulations of Particle Dynamics in a Confined Shear Flow," *AIAA J.* 34(6): 1160-1166 (1996).
- Holman, J.P., *Heat Transfer*, McGraw-Hill, New York, 1981, pp.247.
- Yu, K.H., Trouve, A., and Daily, J.W., "Low-frequency pressure oscillations in a model ramjet combustor," *JFM* 232, 47-72 (1991).
- Poinot, T., Trouve, A., Veynante, D., Candel, S.M., and Esposito, E., "Vortex driven acoustically coupled combustion instability," *JFM* 177, 265-292, (1987).
- Yu, K.H., Wilson, K.J., and Schadow, K.C., "Liquid-Fueled Active Instability Suppression," *Twenty-Seventh Sympo. (Inter.) on Combustion*, The Combustion Institute, Pittsburgh, PA, 1998.



detectors

optical  
fiber



# Laser

## *Solved Mysteries*

To learn more about combustion at the molecular level, scientists at Stanford University are using advanced laser technology to peek inside an engine's chambers. Until recently, the flows generated during the burning process have been difficult to quantify due to the harsh environment presented by an operating engine.

Semiconductor diode lasers that operate in the near infrared range are ideally suited for sensing a range of parameters, such as temperature, velocity, and gas concentrations, because they are rapidly tunable to wavelengths absorbed by the combustion gases. Another important advantage is their compatibility with high-quality fiber optics. The researchers can use off-the-shelf beam splitters to send multiple sensor beams to multiple locations from a single laser source. Information gleaned from the rapidly evolving technology of laser-based sensors may ultimately lead to improved engineering designs for combustion systems. The same technology may also result in better control of combustion and propulsion systems, rendering them more efficient and less polluting. - D.B.



---

# Diode-Laser Absorption Sensors for Combustion Measurements and Control

---

**Ronald K. Hanson and Douglas S. Baer**

*Stanford University*

*Stanford, CA*

---

## Summary

The increasing availability and reliability of lasers over the last 30 years has revolutionized measurement capabilities in research and development laboratories worldwide. In particular, advances over the last decade in semiconductor diode lasers which were developed primarily for fiber-optic telecommunications, computer networks and optical data storage applications, have enabled the development of a new class of gas sensors that may be applied for measurements and control of a wide range of engineering systems. These sensors, comprised of economical and rugged diode lasers and fiber-optic components and based on absorption spectroscopy techniques, are especially promising for non-intrusive, time-resolved, species-selective measurements in hostile environments where the use of conventional probes may be difficult or undesirable. Here we describe the development and application of diode-laser sensors for real-time measurements and active control of combustion and propulsion systems. These same sensors may also be applied to industrial facilities for process control, and for compliance and emissions monitoring.

## Introduction

Over the last twenty-five years, researchers in Stanford University's High Temperature Gasdynamics Laboratory have developed and applied novel absorption diagnostic techniques for measurements of important quantities, including gas concentrations, temperature, velocity, and mass and momentum flux, in laboratory and industrial combustion, propulsion, incineration and hypersonic flows. Quantitative data for these parameters are difficult to obtain by other methods and yet are of extreme importance in characterizing the flows produced in high-temperature or high-speed test facilities. These diagnostic strategies have generally employed continuous-wave (cw) laser sources,

ranging from lead-salt diode lasers (in the 1970's), ring-dye lasers (1980's) and most recently (1990's), near-infrared semiconductor diode lasers. The output wavelength of these sources may be precisely and rapidly controlled (i.e., tuned) to coincide with absorption transitions of specific gases of interest.<sup>1-3</sup> The key limitation of these line-of-sight absorption techniques, the inability to provide full spatial resolution, is generally not significant when probing flows with reasonable or high uniformity (along the measured path). Furthermore, the ability to measure integrated quantities across a flow is often specifically required or highly desirable.

Semiconductor diode lasers operating in the near infrared (IR) are attractive light sources for sensing applications because they are rapidly tunable, small and lightweight, low-cost, efficient, robust, operate at near-ambient temperatures, and produce narrow-bandwidth radiation over a broad wavelength range. Figure 1 presents calculated absorption spectra of important combustion-related gases (including CO, CO<sub>2</sub>, H<sub>2</sub>O, NO, CH<sub>4</sub>, O<sub>2</sub>) in the spectral region currently accessible using room-temperature semiconductor diode lasers (0.6-3.0 microns) to illustrate the range of important gases that may be probed at present. In general, careful selection of the probe wavelength will allow the measurement of a single species (gas) and avoid cross-sensitivity effects which are difficult to exclude with conventional sensors (electrochemical cells) or low resolution absorption-based systems (non-dispersive infrared detection systems).

Perhaps the most significant advantage in the use of near-IR diode lasers is their compatibility with rugged, communications-grade fiber-optic hardware. Fiber optics may be used to combine (i.e., *multiplex*) the outputs of multiple lasers at different wavelengths into a single probe beam, and thus allow simultaneous measurements of temperature and the concentrations of multiple species along a single optical

path. Moreover, the resultant multi-wavelength probe beam may be subsequently divided into several paths using inexpensive off-the-shelf fiber-optic splitters, and thus allowing measurements of temperature and species concentrations in multiple locations simultaneously, with only a single set of laser sources. Since the lasers presently represent the most expensive component of this measurement system, the use of fiber optics can thus dramatically reduce the cost per measurement location. The combination of fiber-optic and diode-laser technology with laser-absorption spectroscopy techniques can provide a compact, rugged and economical sensor system for species-specific measurements that are insensitive to interferences, particulates, and background luminosity. These qualities make diode-laser sensors ideal for process control in a variety of hostile environments, including combustion and propulsion flows, as well as industrial process streams.

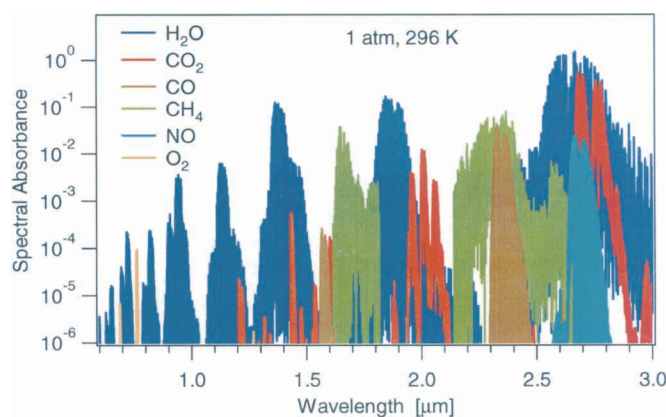


Fig. 1 – Calculated absorption spectra of important combustion gases in the 0.6-3.0 micron spectral region that is currently accessible using room-temperature semiconductor diode lasers. The calculations use a 10% mole fraction for each gas, 296-K temperature, 760-torr total pressure, and 1-cm path length.

In this work, we describe recent work by Stanford researchers in the development and application of diode-laser sensors for measurements in and control of pulsed combustion facilities at the Naval Air Warfare Center at China Lake (NAWC) for shipboard incineration and at the Naval Postgraduate School (NPS) at Monterey for an advanced propulsion system (pulse detonation engine). These measurements performed in high-temperature, high-pressure, time-varying flows, underscore the potential of diode-laser sensors for process control of hostile environments where conventional probes and measurement techniques are inappropriate or ineffective.

## Measurement Principles

The measurement principle for diode laser sensors is based on the absorption of laser light at a particular wavelength (i.e., color) by a specific gas of interest. In brief, the laser

radiation induces the molecule to undergo a transition from an initial quantum state to a final state, which corresponds to a particular vibration-rotation transition. The laser wavelength corresponds to the energy difference between the initial and final quantum states. The magnitude of the absorption is related to the population of molecules in the absorbing state, as described by statistical mechanics and is a function of temperature. Furthermore, the shape and relative position of an absorption feature is related to local environmental effects such as temperature and pressure through Doppler and pressure broadening, respectively, and is affected by the gas velocity through the Doppler shift. Spectrally resolved absorption measurements can exploit these dependencies to allow simultaneous determinations of multiple gasdynamic parameters.

The transmission of light directed through a flowfield may be described using the Beer-Lambert relation

$$T_v \equiv \frac{I_v}{I_0} = \exp(-k_v L)$$

where  $T_v$  is the fractional transmittance of the medium at frequency  $\nu$ ,  $I_0$  is the incident intensity of the laser beam,  $I_v$  is the intensity after propagation through a length  $L$  [cm] of the absorbing medium, and  $k_v$  [ $\text{cm}^{-1}$ ] is the absorption coefficient at frequency  $\nu$ . The absorption coefficient is a function of the total pressure,  $P$  [atm], the mole fraction of absorbing species,  $\chi$ , species-specific spectroscopic parameters, and the gas temperature. At a fixed wavelength and a constant temperature and pressure, the absorption coefficient is proportional to the probed species mole fraction. The gas temperature may be determined from measurements of the transmission intensity at two selected wavelengths, or from the shape of an absorption line dominated by Doppler-broadening effects. The appropriate line pairs for thermometry may be determined *a priori* from known spectroscopic parameters for a particular gas. The partial pressure (and concentration if the pressure is known) of a particular gas can be inferred from the measured absorption and temperature. For measurements of weakly absorbing gases, i.e., where  $k_v$  is small, measurement sensitivity may be improved by increasing the path length using folded-path optical arrangements if necessary. Furthermore, measurements of the magnitude, shape and shift of an absorbance feature may enable determination of velocity, as we have demonstrated in arcjet thrusters<sup>4</sup> (where velocities reach  $V \approx 15$  km/s) and hypersonic test facilities<sup>5</sup> (Mach numbers of 16 have been monitored), and of electron number density and temperature<sup>6</sup> (up to 15,000 K), as demonstrated in atmospheric pressure plasmas and shock tubes.<sup>7</sup>

## Measurements in Forced Combustion Systems

Multiplexed diode-laser absorption sensors were applied to measure and control gas temperature and  $\text{H}_2\text{O}$  concentration

in the combustion region of an experimental (50-kW) pulsed annular dump combustor.<sup>8</sup> This combustor serves as a model of an afterburner in a compact, multi-stage, waste incineration system under development at the Naval Air Warfare Center (NAWC) at China Lake (California) for use aboard Navy ships. The concentrations of important pollutants and unburned fuel constituents (e.g., CO, C<sub>2</sub>H<sub>2</sub>, C<sub>2</sub>H<sub>4</sub>) were also monitored on line in the exhaust stream.

A schematic diagram of the NAWC multi-stage incineration concept including diode laser sensors for real-time control is illustrated schematically in Figure 2. The incinerator

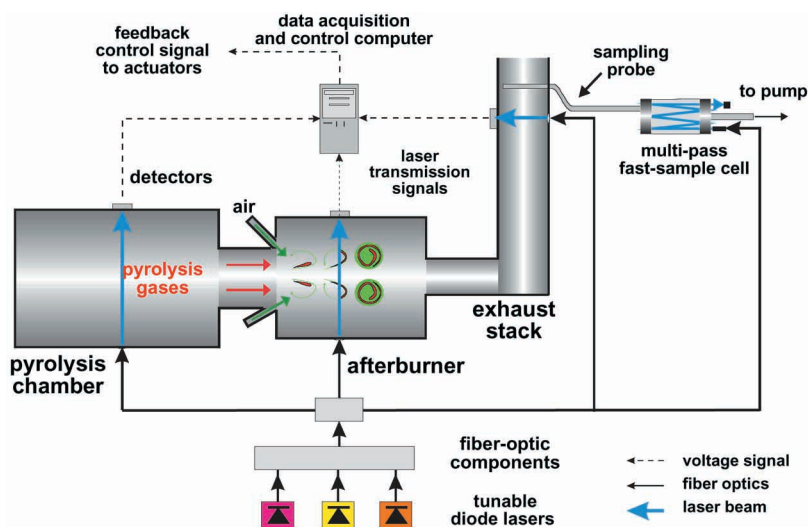


Fig. 2 – Schematic diagram of the setup for measurements in and control of a multi-stage waste incineration system using diode-laser sensors.

converts solid waste to gaseous waste using a starved-air pyrolysis chamber and then removes the hazardous components using a secondary oxidation chamber or afterburner that utilizes the concepts of forced vortex combustion for a compact and efficient design. Details of the afterburner, including the design, application of advanced diagnostics, and determination of the destruction and removal efficiency (DRE) for both small- and large-scale systems may be found in the references.<sup>9-11</sup>

The strategy for increasing the combustion efficiency in the afterburner involves acoustically forcing (modulating) the input fuel and air to generate stabilized vortices which allow for rapid and controlled mixing of the air and pyrolysis gases. The result of better mixing is more efficient and complete combustion and less pollution, which allows the construction of smaller incineration systems onboard ships where space is a premium. However, full exploitation of this forced combustor technology has required the development of real-time sensing and fast active control. The real-time measurements in the combustion and exhaust regions of the afterburner combined with active control strategies demonstrate the utility of diode-laser sensors for realistic engineer-

ing applications including performance assurance and compliance monitoring.

Figure 3 presents photographs of the (5-kW) laboratory-scale combustor at Stanford and the (50-kW) combustor at NAWC that served as experimental test beds for the development of diode-laser sensors for combustion measurements and control. The combustors were operated on C<sub>2</sub>H<sub>4</sub>, which served as a waste surrogate, and air for these projects.

For *in situ* combustion measurements, two independently operated diode lasers were tuned repetitively over the desired H<sub>2</sub>O transitions (vibration-rotation transitions in the 2v<sub>1</sub> and v<sub>1</sub> + v<sub>3</sub> vibrational bands) to yield absorption measurements at both 1343 nm and 1392 nm every 300 microseconds. The individual laser outputs were combined into a single path using fiber splitters and couplers. An optical fiber delivered the multi-wavelength beam to the combustor and a GRIN lens fused to the end of the fiber collimated the light through the flowfield. The transmitted multi-wavelength light was de-multiplexed (spectrally separated) into the constituent laser wavelengths by directing the beam onto a diffraction grating. The beams were diffracted at angles specific to each wavelength and were subsequently monitored with photodiodes. The voltage signals from the photodiodes were then sent to a personal computer for analysis and to determine the appropriate feedback control signal. Temperature was determined from the ratio of measured peak absorbances at each wavelength. Water-vapor mole fraction was

determined from the measured absorbance of a single transition and the gas temperature. The measurements were recorded, analyzed and an updated feedback control signal was sent to the actuator at a 3-kHz rate.

For these forced combustion systems, a strong correlation was established between the *magnitude* of the measured temperature oscillations (i.e., T<sub>rms</sub>) in the combustion region and the measured concentrations of CO and hydrocarbons in the exhaust. The expectation, confirmed by experiment, is that higher temperature oscillations correspond to more complete combustion (and hence higher energy release and higher peak temperatures) in the burning vortices of fuel and air which pass by the monitoring station. Consequently, adaptive control strategies were developed to maximize the temperature oscillations by continuously adjusting the relative phase between the acoustically driven (modulated) fuel and air flows.

As an example, figure 4a presents measurements and control of gas temperature in the combustion region of the NAWC incinerator. Large coherent temperature oscillations at the forcing frequency (T<sub>rms</sub>) are prominent when control is



applied and the phase between the fuel and air flows is optimized. The time response of the control strategy is presented in Figure 4b. The optimum phase value was reached in approximately 100 milliseconds, illustrating the rapid response of the measurement and control strategies. It is the uniquely fast response of the diode-laser sensors, coupled with clever algorithms and fast actuators, which enables this significant reduction in system control time.

For on-line measurements of combustion emissions, a fast extractive-sampling method was developed for sensitive detection of pollutants and unburned fuel (e.g., CO, CO<sub>2</sub>, CH<sub>4</sub>, C<sub>2</sub>H<sub>4</sub>, and C<sub>2</sub>H<sub>2</sub>) in the combustor exhaust. For these measurements, post-combustion exhaust gases were sampled continuously with a water-cooled stainless-steel probe (4-mm internal diameter) with several inlet holes (0.5-mm diameter). The gases were directed into a compact (0.3-liter volume) multi-pass (folded optical path) cell which consists of two mirrors with a 20-cm separation and a 33-meter absorption pathlength. Accurate species concentrations in

sampled gases flowing through the cell were determined from measured absorbances with response times on the order of a few seconds. Faster response times may be obtained by increasing the pump speed and decreasing the length of tubing from the sampling probe to the measurement cell.

For these exhaust emissions measurements, two fiber-coupled distributed feedback (DFB) diode lasers operating near 1.64  $\mu\text{m}$  and 1.66  $\mu\text{m}$ , and an external cavity diode laser (ECDL) with a wavelength tuning range of 1.49–1.58  $\mu\text{m}$  were used. The DFB laser was wavelength-tuned over the selected CH<sub>4</sub> and C<sub>2</sub>H<sub>4</sub> transitions for measurements of unburned fuel. The tuning range of the ECDL spanned

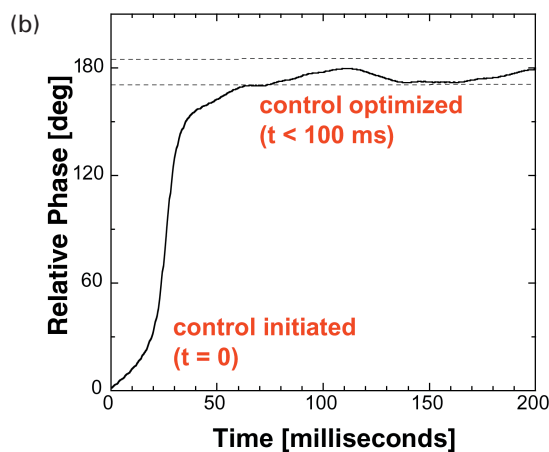
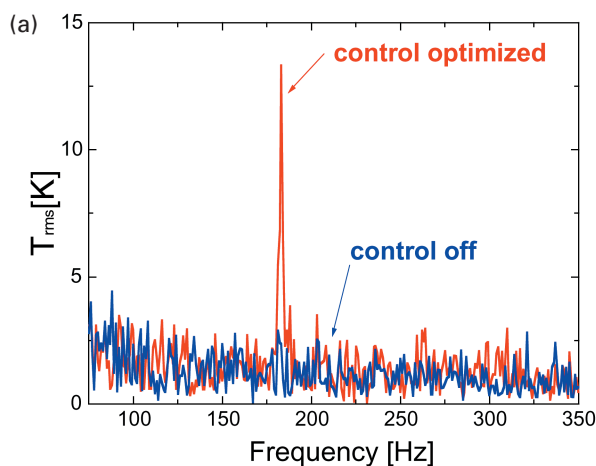
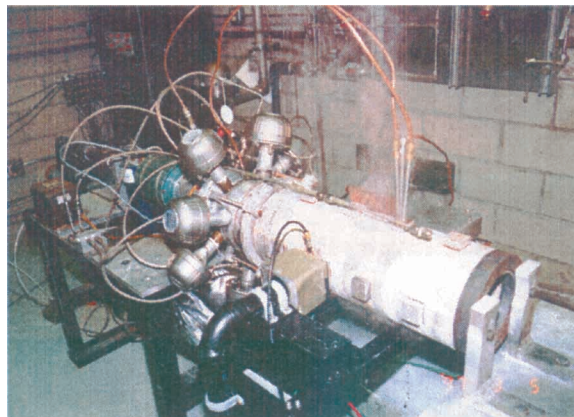


Fig. 4 – Measurements and control of temperature in the combustion region of the forced incinerator at NAWC China Lake. Large coherent temperature oscillations at the desired frequency ( $T_{rms}$ ) correspond to efficient mixing and optimized combustion (a). Time response of the control strategy using the diode-laser-based temperature measurements as input and the relative phase between the acoustic forcing of the fuel and air flows in the combustor as a control variable (b).

Fig. 3 – Photographs of the acoustically forced combustors at Stanford, left, and NAWC China Lake, below, for development of diode-laser sensors for combustion measurements and control. [Facilities courtesy of Drs. T. Parr and K. Schadow at NAWC]



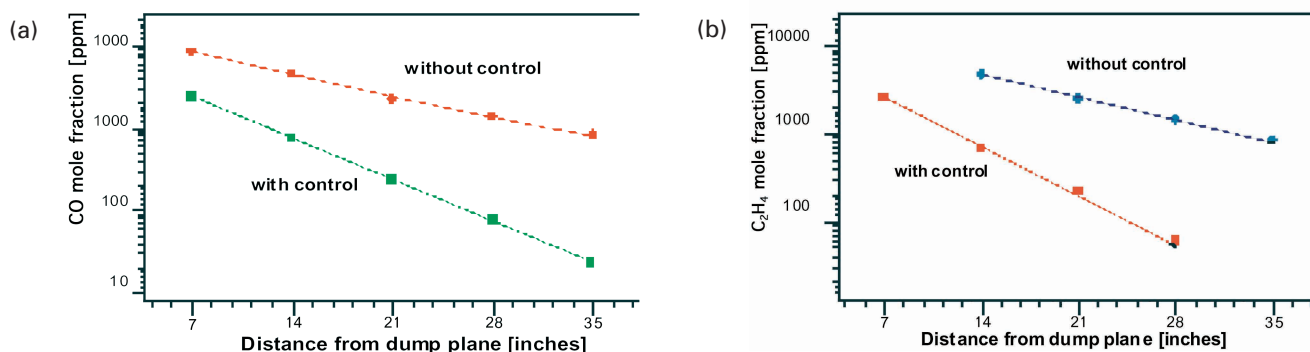


Fig. 5 – Measurements of CO (a) and C<sub>2</sub>H<sub>4</sub> (b), i.e., unburned fuel, using diode-laser sensors in the forced incinerator at NAWC China Lake with and without active combustion control. [Facility courtesy of Dr. T. Parr and Dr. K. Schadow]

various CO, CO<sub>2</sub>, and C<sub>2</sub>H<sub>2</sub> transitions for measurements of unwanted pollutants. The laser outputs were combined into one optical fiber using a fiber combiner. The beams were directed through the multi-pass absorption cell and focused at the exit onto a photodetector. The transmission signals were transferred to a personal computer for real-time determination of species concentrations. The system may be easily expanded to other important species (e.g., NO) as lasers become available at the required wavelengths.

Figure 5 illustrates measurements of CO and C<sub>2</sub>H<sub>4</sub> (as unburned fuel) at various distances from the combustion region with and without active combustion control. The decrease in the CO and C<sub>2</sub>H<sub>4</sub> concentrations and the increase in the rate of destruction of CO and C<sub>2</sub>H<sub>4</sub> with control validates the forced-combustion scheme for compact incinerators and illustrates the utility of the laser-sensor measurement and control strategy.

## Measurements in Advanced Propulsion Systems

Research and development of advanced propulsion systems is a particularly attractive target for diode-laser sensing owing to the need for accurate species and temperature data with high specificity and rapid response in a very hostile environment. A system of current interest to the Navy is the pulse detonation engine (PDE) which is under study at the Naval Postgraduate School (NPS) and elsewhere. Here we report early work by Stanford researchers to extend and apply diode-laser sensors for measurements of gas temperature and species concentrations in a PDE facility at NPS.

An air-breathing pulse-detonation engine offers the potential for providing long range, high cruise speed and subsonic loiter, and in principle, can provide high performance with fewer moving parts and lower cost. The rapidly varying flows generated by pulse detonation engines create challenging environments for sensors due to the high pressures (can exceed 100 atm) and temperatures (approaching 4000 K) and

the presence of soot and liquid-fuel droplets, and yet detailed measurements of the type possible with tunable diode lasers are critically needed to facilitate development of reliable, efficient propulsion systems. Under these conditions, the duration of a single pulse is on the order of a millisecond or less and absorption features are broadened considerably. Furthermore, at combustion temperatures soot generates strong blackbody emission that can complicate analysis of the laser transmission signals, and soot and liquid fuel droplets can contribute to the extinction of the probe beam that must be distinguished from molecular absorption. Density gradients tend to refract beams propagating through

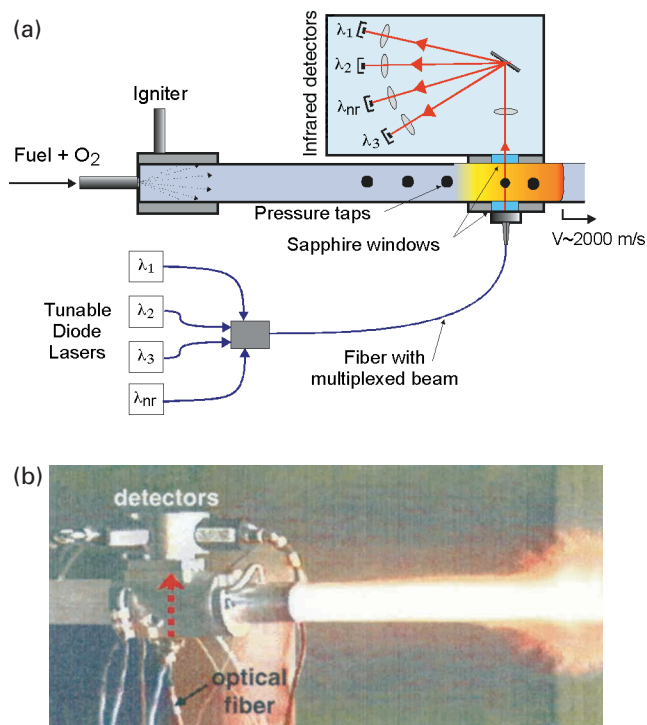


Fig. 6 – Schematic diagram of the setup for diode-laser diagnostics (a). Photograph of the PDE facility at NPS during exhaust (b). [Courtesy of Profs. David Netzer and Chris Brophy]

the flow (often called beam steering) and stress-induced birefringence at optical ports (windows) can affect (or modulate) the transmitted laser intensities. Moreover, since reliable spectroscopic data at elevated temperatures and pressures are sparse, there is a strong need for basic spectroscopic studies of key species in order to allow quantitative use of diode laser absorption. Finally, the rapidly changing conditions in PDE flows demand fast measurements and high-bandwidth detection to enable the desired temporal resolution to accurately describe the flowfield.

A schematic diagram of the experimental setup for measurements in PDE flows is shown in Figure 6a. Fuel and oxygen are injected and ignited at the head end of the tube. The detonation wave builds and travels toward the tail end of the tube at approximately the Chapman-Jouget velocity ( $V_{\text{wave}} \approx 2$  km/s) for a detonation wave. Several optical diagnostics of the type described here can be installed along the length of the detonation tube; only one is shown for simplicity.

Light from each of four diode lasers operating in a remote control room is combined (multiplexed) and carried to the PDE via communications-grade optical fiber. The multiplexed beam is passed through windows in the facility, demultiplexed by a lens-grating system, and detected by appropriate photodetectors. In addition to demultiplexing the four wavelengths, the grating serves to reduce blackbody emission sensed by the detectors. The entire demultiplexing and detection system is purged with dry nitrogen gas to eliminate absorption due to the natural presence of room water (humidity).

The wavelengths of the four diode lasers were tuned to the peaks of three water-vapor absorption features ( $\lambda_1 = 1.34$   $\mu\text{m}$ ;  $\lambda_2 = 1.39$   $\mu\text{m}$ , and  $\lambda_3 = 1.80$   $\mu\text{m}$ ) and to a non-resonant wavelength ( $\lambda_{\text{nr}} = 1.65$   $\mu\text{m}$ ) to account for laser extinction due to soot and liquid fuel droplets. All beams follow the same optical path through the flow and are subsequently monitored using individual photodetectors. The collection system was designed to be insensitive to deflections in the beams due to refractive effects.  $\text{H}_2\text{O}$  is the target species for this diagnostic since it is a major combustion product and the strongest absorber within the wavelength range of currently available diode lasers.

Preliminary data were recorded in a 1.5-inch diameter pulse detonation tube operating on liquid JP-10 /  $\text{O}_2$  at the Naval Postgraduate School. This tube serves as the initiator for a larger (6") diameter PDE and has been extensively characterized. A photograph of the facility during detonation and exhaust of unburned gases is shown in Figure 6b. The luminosity is predominantly due to soot emission that results from incomplete combustion of the liquid JP-10 fuel.

Data taken during a single pulse of the NPS detonation tube are shown in Figure 7a. The pressure trace is from a transducer located at the same axial location as the diode-laser sensor. The measured absorbance versus time was obtained for each of the three water transitions (only one wavelength shown for clarity). Values of gas temperature were determined from two-line ratio of  $\text{H}_2\text{O}$  absorption and from two-color soot pyrometry (not shown in Fig. 6). The water mole

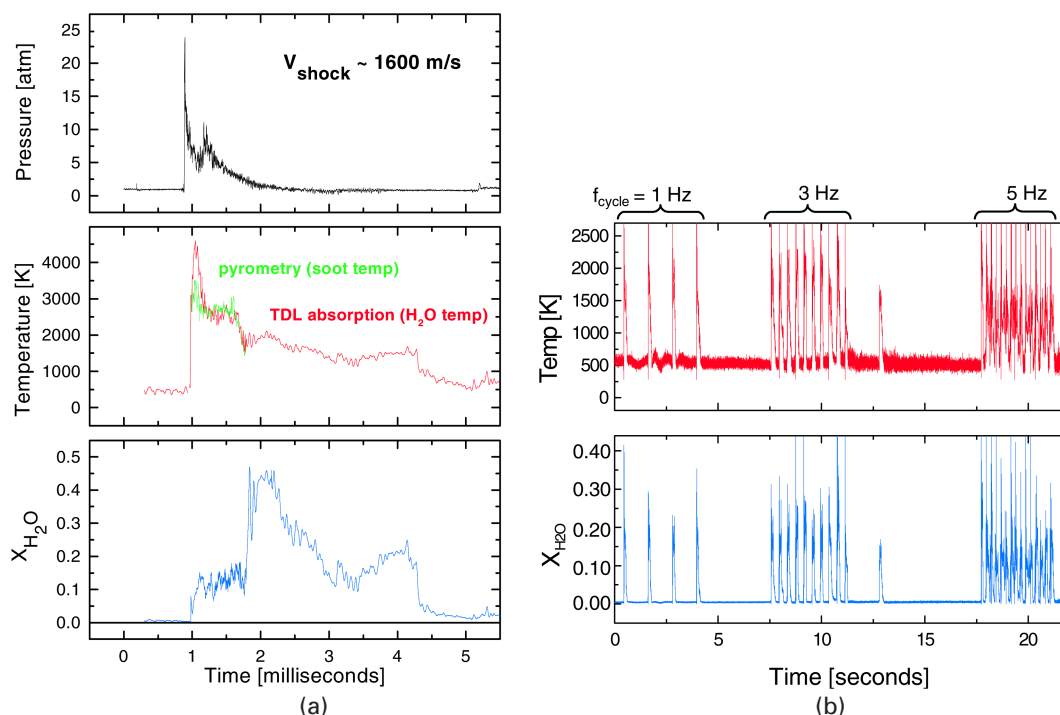


Fig. 7 – Measurements of pressure, gas temperature, soot temperature, and water vapor recorded in a single pulse (a); and temperature and  $\text{H}_2\text{O}$  during repetitive pulses at different firing rates using diode-laser sensors and emission diagnostics in the PDE facility at NPS (b).



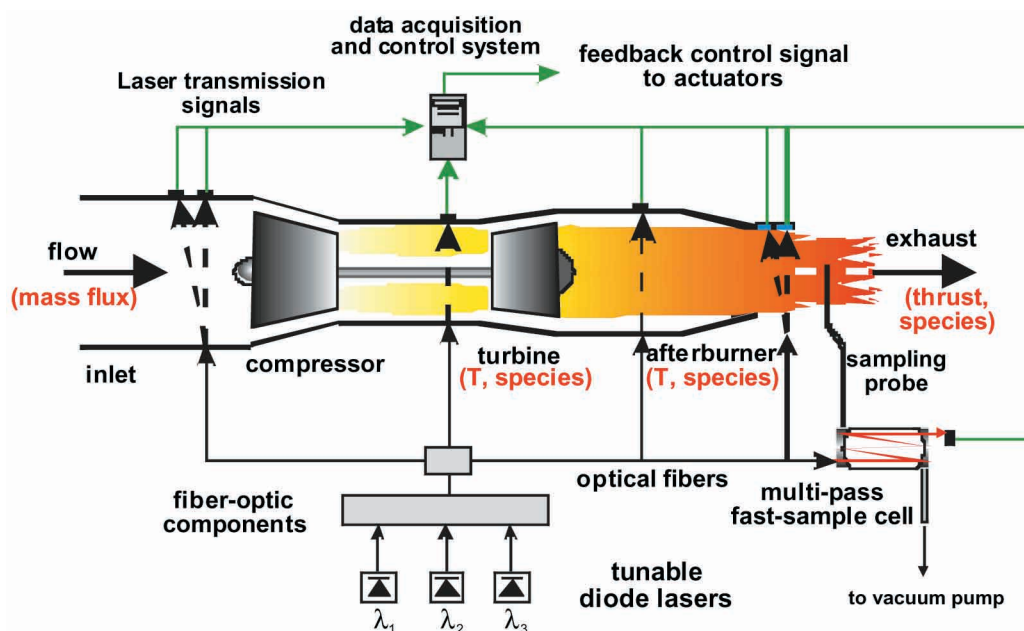


Fig. 8 – Schematic diagram of the setup for real-time control of aero-propulsion gas turbines using diode-laser sensors for *in situ* and extractive sampling measurements. Gas parameters that may be measured at the specified locations are listed in red.

fraction was determined from the measured values of  $H_2O$  absorbance, temperature, and pressure.

The TDL absorption diagnostic provides many insights that were not previously attainable with traditional sensors. For instance, although the pressure trace suggests that the flowfield becomes relatively quiet during the first millisecond following the detonation pulse, the diode laser sensor shows a strong increase in water mole fraction near  $t=1.8$  milliseconds. This increase corresponds to an expansion wave traveling from the exit to the head end after the detonation wave leaves the tube.

Figure 7b presents continuous values of temperature and water mole fraction during pulse detonation rates of 1, 3, and 5 Hz. The advantages to fast, continuous monitoring are apparent. For instance, the data show that at a 5-Hz firing rate, a cycle's post-detonation exhaust is not completed before the fill and ignition of the following cycle. This effect may explain why this particular tube was unable to detonate reliably near or above a 5-Hz rate. Information of this kind will likely play an important role in the development and optimization of PDE systems with high repetition rates.

We anticipate that additional measurements with higher accuracy and including other species (candidates include OH, CO, and unburned hydrocarbons) will be obtained as the diagnostic is applied to both the NPS facility and the Stanford PDE facility currently under construction. In addition, velocity measurements based on Doppler shifts of absorption features are planned to enable direct, time resolved measurements of exhaust velocity and thrust, the most important parameter for propulsion systems. The diagnostic promises to enhance detailed modeling of PDE

flows and, eventually, enable active closed-loop control of the PDE.

## Future

Continuing advances in semiconductor and communications technologies over the next decade will almost certainly add momentum to the further development of laser-based sensors, well-suited for real-time monitoring and process control of combustion and propulsion systems. These sensors, comprised of semiconductor diode lasers and fiber-optic components, and based on absorption spectroscopy techniques, already hold significant potential for measurements of key gas parameters inside *realistic* combustion facilities and present the opportunity of novel system control strategies not previously considered. Figure 8 illustrates our vision of the potential of diode-laser sensors for measurements and control of multiple parameters (including temperature, velocity, concentrations, mass flux and thrust) in gas turbine aero-propulsion systems. In addition, these same sensors will serve as important diagnostic tools to allow improved understanding of chemical and physical processes that govern the operation of these systems, thus enabling improved design and development of next-generation facilities. As new and more broadly tunable diode-laser sources become available, based on novel designs and semiconductor materials currently under development, access to the ultraviolet and infrared spectral regions will be enabled and this will lead to significant new opportunities for sensitive measurements of additional species and with increased sensitivity. The growing use of lasers for sensing and control of combustion and propulsion systems is thus almost a certainty.

---

## Acknowledgments

This work was sponsored by the Office of Naval Research with Drs. Gabriel Roy and Klaus Schadow as technical monitors. Partial support from the U.S. Air Force Office of Scientific Research, Aerospace Sciences and Materials Directorate, with Dr. J. Tishkoff as technical monitor, is also gratefully acknowledged.

## Biographies

For the biography of **Ronald Hanson**, see Profiles in Science on the inside back cover.

**Douglas Baer** received his undergraduate education in Engineering Physics at the University of California, Berkeley (B.S. 1982). Following 18 months as a Research Associate at the Desert Research Institute, Ben Gurion University, Israel, he earned graduate degrees in Mechanical Engineering at the High Temperature Gasdynamics Laboratory (HTGL) at Stanford University (M.S. 1985, Ph.D. 1993) under the guidance of Professor Ron Hanson. From 1993 through 1999, Dr. Baer was affiliated with the Department of Mechanical Engineering at Stanford University as a postdoctoral Research Scientist in the High Temperature Gasdynamics Laboratory. Dr. Baer is currently with Informed Diagnostics, Inc.

## References

1. R. K. Hanson, P. A. Kuntz and C. H. Kruger, "High-Resolution Spectroscopy of Combustion Gases Using a Tunable Infrared Diode Laser," *Applied Optics* **16**, 2045-2048 (1977).
2. E. C. Rea, Jr., S. Salimian and R. K. Hanson, "Rapid-Tuning Frequency-Doubled Ring Dye Laser for High Resolution Absorption Spectroscopy in Shock-Heated Gases," *Applied Optics* **23**, 1691-1694 (1984).
3. R.K. Hanson, D.S. Baer, C. Morris, M. Thurber, E. Furlong and S. Wehe, "Recent Advances in Laser-Based Diagnostics for Gaseous Flows," invited plenary paper, SPIE/VSJ, Yokohama, December 7-9, 1998; also *J. Visualization* **2**, No. 3/4 (1999).
4. R.J. Cedolin, W.A. Hargus Jr., P.V. Storm, R.K. Hanson and M.A. Cappelli, "Laser-Induced Fluorescence Study of a Xenon Hall Thruster," *App. Phys. B*, **65**, 459-469 (1997).
5. S.D. Wehe, D.S. Baer and R.K. Hanson, "Tunable Diode-Laser Absorption Measurements of Temperature, Velocity and H<sub>2</sub>O in Hypersonic Flows," paper AIAA-97-3267 at 33<sup>rd</sup> Joint Propulsion Conference, July 7-9, 1997, Seattle, WA.
6. D. S. Baer and R. K. Hanson, "Tunable Diode Laser Absorption Diagnostics for Atmospheric Pressure Plasmas," *Jour. of Quant. Spectrosc. and Radiative Transfer* **47**, 455-475 (1992).
7. H.A. Chang, D.S. Baer, and R.K. Hanson, "Semiconductor laser diagnostics for simultaneous determination of kinetic and population temperatures in high-enthalpy flows," 19<sup>th</sup> International Symposium on Shock Waves, Marseilles, France (1993).
8. E.R. Furlong, R.M. Mihalcea, M.E. Webber, D.S. Baer and R.K. Hanson, "Diode Laser Sensor System for Closed-Loop Control of a 50-kW Incinerator," paper AIAA-97-2833 at 33<sup>rd</sup> Joint Propulsion Conference, July 7-9, 1997, Seattle, WA.
9. T.P. Parr, E.J. Gutmark, K.J. Wilson, D. M. Hanson-Parr, K. Yu, R.A. Smith, and K.C. Schadow. *Twenty-Sixth Symposium (International) on Combustion*, p. 2033-2055, The Combustion Institute, Pittsburgh, 1996.
10. T.P. Parr, K.J. Wilson, K. Yu, R.A. Smith, and K.C. Schadow. *15th International Conference on Incineration and Thermal Treatment Technologies*, May 1996, Savannah, GA.
11. E.R. Furlong, D.S. Baer and R.K. Hanson, "Real-Time Adaptive Combustion Control Using Diode-Laser Absorption Sensors," 27<sup>th</sup> Symp. (International) on Combustion, The Combustion Institute, pp. 103-111 (1998).







# Going with the

# Coflow



The applications of thrust-vectoring are obvious. The AV-8B *Harrier* is a combat star, and it achieves its extraordinary performance through its thrust-vectoring engines. Short or even vertical take-off and landing capabilities are invaluable, especially to aircraft that operate from ships, or from small, damaged, or improvised airfields. Thrust-vectoring can compensate for loss of aerodynamic lift, and help a pilot keep an aircraft under control during stall conditions.

But thrust-vectoring in operational craft has always come at a high price in terms of mechanical complexity and weight. Gimballed engines or elaborate systems of vents and louvers impose all the usual penalties of moving parts. They are also heavy, and weight is always at a premium in aerospace engineering. If there were a way of altering the direction of a reaction engine's thrust without these mechanical impediments, that would change everything.

Strykowski and Krothapalli describe a fluidic approach to thrust-vectoring that overcomes these disadvantages. It turns out that there are indeed ways of using the fluids present in the system to direct the jets that provide thrust. - J.P.

---

# Vectoring Thrust Using Confined Shear Layers

---

**P. J. Strykowski**

*University of Minnesota  
Minneapolis, Minnesota*

**A. Krothapalli**

*Florida A&M University and Florida State University  
Tallahassee, Florida*

## Abstract

A fluidic scheme is described which exploits a confined countercurrent shear layer to achieve multiaxis thrust vector response of high speed jets in the absence of moving parts. Continuous control of the thrust vector angle is demonstrated in jet exhaust up to Mach 2 for nozzle geometries including rectangular and axisymmetric cross sections. Studies conducted jointly between Florida State University and the University of Minnesota indicate that thrust vector angles up to at least  $20^\circ$  can be achieved at slew rates in excess of 180 degrees per second in laboratory scale nozzles. Complementary studies carried out at China Lake Naval Air Warfare Center on large scale hardware (ten fold laboratory scale) and at high temperatures (over  $3000^\circ\text{F}$ ) suggest that scaling and temperature issues will not preclude the fluidic approach from working. In both studies, secondary mass flow requirements for control were found to be less than approximately 2% of the primary jet mass. The confined shear layer is susceptible to both attached and unattached flow regimes, the nature of which will be discussed. Finally, the performance of the fluidic approach will be examined in the presence of external coflow to evaluate the potential of the concept under flight conditions.

## Introduction

The ability to redirect the thrust of an aircraft engine or rocket exhaust offers several advantages to the aerospace industry. It provides the potential for a vertical component of thrust which may be used, especially at low speeds, to augment the lift force generated by the wings. This allows

the aircraft to take off in a shorter distance, and ascend at a higher rate. During landing, vectored thrust can be used to supplement the lift force generated by the wings, and approach speeds may be reduced without changing the rate of descent. The benefits of short take off and landing aircraft are especially attractive for landing on aircraft-carriers or on damaged airfields. Traditionally the wings are the sole mechanism for generating lift. However they have aerodynamic limitations, namely airfoil stall, which causes a dramatic decrease in airfoil performance and must be avoided to maintain adequate control of the aircraft. Thrust vectoring can be used to maintain or re-establish control under stalled conditions, thus enhancing the overall maneuverability of the plane. In missile applications, multiaxis thrust vector control could be employed for steering control at potentially considerably lower expense in terms of vehicle weight and cost.

There are various methods to vector the exhaust thrust of a jet engine or missile system. One way is to tilt the entire exit plane of the nozzle. While this generally requires complex actuation hardware, it has been implemented successfully on the Harrier jet for years. For vertical take-off the thrust is directed almost fully downwards, and once in flight the nozzle locks in place horizontally and the plane performs in a conventional manner. Another method which has been employed on the Lockheed X-31 and the NASA F-18 High Alpha Research Vehicle, among others, employs hinged turning vanes downstream of the nozzle exit. The exhaust impinges on these mechanically actuated vanes and is deflected. This method has proven to greatly enhance the maneuverability of the test aircraft, as well as considerably



shorten take-off and landing distances. However, these advantages come at the expense of additional weight and reduced thrust due to the wall interaction. Similar advantages can be achieved, in principle, without intricate mechanical control systems and with improved thrust recovery, by fluidically vectoring the jet.

The present study concerns a method of fluidic vector control which employs a confined countercurrent shear layer. This approach, also known as Counterflow Thrust Vector Control, or CF-TVC, attempts to combine the continuous and proportional features of mechanical based systems with the simplicity of fluidic control, and has recently been demonstrated experimentally for both subsonic and supersonic jets.<sup>1,2</sup> Successful fluidic vectoring must achieve proportional and non-hysteretic control over a significant portion of the operation envelop, while minimizing the secondary mass flow required for actuation. The basic concept of counterflow thrust vectoring can best be illustrated by referring to the sketch in Figure 1a, where the side view of the short dimension of a rectangular jet is shown. The primary jet exhausts from the nozzle between symmetric curved surfaces called *collars*, placed on either side of the primary stream. To achieve upward thrust vectoring at an angle  $\delta_v$ , a secondary counterflow must be established in the upper shear layer of the jet. This can be accomplished by applying suction to the plenum chamber located between the upper curved surface and the primary nozzle. The action of

counterflow in the upper shear layer gives rise to asymmetric entrainment and a cross-stream pressure gradient sufficient to vector the jet.

The ability of the jet to vector in the presence of a stationary surface has been commonly referred to as the Coanda effect.<sup>3</sup> As a nominally two-dimensional jet issues from the nozzle, the shear between the jet and the surrounding quiescent fluid gives rise to lateral momentum transport which is accentuated by the turbulent mixing of the shear layer. This process leads to momentum mixing between the two fluids and is commonly referred to simply as entrainment. Because the jet is gathering fluid through entrainment, its boundaries diffuse outward and, in the process, weaken the jet's ability to further entrain the surrounding fluid. Figure 1b depicts the two-dimensional jet with a curved surface of radius  $R$  aligned tangentially to the edge of the nozzle exit. The fluid entrained along the lower collar surface by the pumping action of the shear layer is constrained, giving rise to subatmospheric pressures in that region. This differential pressure draws the jet toward the curved surface. It is this change in the pressure field within the vicinity of a solid surface that is known as the Coanda effect. (First described by Young,<sup>3</sup> the Coanda effect is named for the French engineer who patented the "effect" in 1932.) If the entrainment rate is sufficiently high, the pressure continues to drop until the jet becomes attached to the surface. It is this attachment process that is most often associated with the Coanda effect. However, attachment is not a necessary condition for the Coanda effect, but rather a consequence of it.

Once the flow becomes attached, the jet continues to entrain fluid between itself and the curved surface leading to further wrapping of the jet around the surface. This process continues until the shear layer structures have weakened sufficiently and can no longer entrain the fluid necessary to force the jet against the surface. The point of separation of the jet from the surface is therefore dependent on the nature of the shear layer structures and their ability to entrain ambient fluid. Once the jet has established itself in the configuration shown in Figure 1b under steady conditions, it remains stable, i.e., perturbations to this flow result in the jet reestablishing itself to the condition prior to the perturbation. While the attached portion of the jet is obviously no longer entraining fluid against the curved wall, the pressure there is kept low as demanded by the equations of motion. Under these conditions, the curved jet can be described by two-dimensional cylindrical coordinates  $r$  and  $\theta$  which, respectively, are the local radius of the curved jet and its angular position. The corresponding local velocities in the  $r$  and  $\theta$  directions are then  $u_r$  and  $u_\theta$ . If we assume that the flow is nominally parallel in the vicinity of the collar, namely that  $u_\theta = u_\theta(r)$  and  $u_r = 0$ , we obtain for a steady, inviscid and incompressible fluid the following relationship:

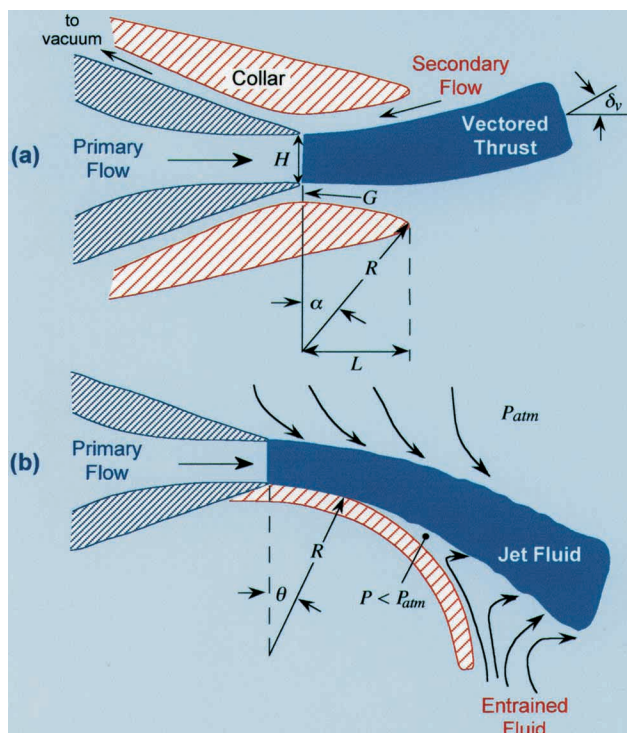


Fig. 1 – (a) Schematic of fluidic thrust vectoring nozzle when counterflow is activated in the upper shear layer of the jet; (b) jet attachment to a curved surface caused by natural entrainment commonly referred to as the Coanda effect.



$$\frac{\partial P}{\partial r} = \frac{\rho u_{\theta}^2}{r} \quad (1)$$

Consequently, the pressure gradient in the r-direction is seen to increase with the square of the velocity. Therefore, the pressure will increase from some minimum value at the curved surface to atmospheric pressure near the outer boundary of the jet, ensuring that the centripetal acceleration is balanced by the pressure field.

The distribution of vacuum pressure maintained on the curved surface will determine the net forces acting on the surface. However, one of the inherent difficulties of controlling the Coanda effect as described above, is its passive nature. For a given jet momentum flux and nozzle-collar geometry, a fixed pressure distribution will be created on the collar, and therefore a fixed side force will be generated. Hence, the Coanda effect leads to hysteretic jet attachment and bistable operation, which could be used for thrust vector control if the Coanda surface were designed to be movable. But this configuration would defeat the initial attractiveness of fluidic control using stationary hardware, and hence why the passive Coanda effect as shown in Figure 1b was not examined as a likely candidate for aircraft and missile control applications. However, if the jet curvature can be controlled by, for instance, manipulating jet entrainment, the cross stream pressure field can be altered *continuously*, and thereby generate the side forces necessary to vector thrust and avoid hysteresis.

Strykowski, Krothapalli & Jendoubi<sup>4</sup> demonstrated that counterflow, when applied to the periphery of an axisymmetric jet, greatly enhanced the entrainment characteristics of the shear layer. By applying counterflow on only one side of the jet, the excited shear layer entrains mass more effectively than the opposing free shear layer. This imbalance in entrainment causes a cross-stream pressure gradient, which deflects the jet in the direction of the applied counterflow, resulting in a vectored primary flow. Van der Veer & Strykowski<sup>1</sup> were able to proportionally pitch vector control a subsonic rectangular jet up to Mach 0.5 at angles up to 20°. Strykowski, Krothapalli & Forliti<sup>2</sup> achieved similar pitch vectoring performance in a supersonic jet at Mach 2.

No moving parts are directly required to steer the jet when CF-TVC is employed. Consequently, reliability can, in principle, be greatly enhanced. Furthermore, there are no surfaces in direct contact with the high temperature, high velocity exhaust gases. This may eliminate the need for expensive materials or exotic cooling schemes, which would be necessary with turning vanes. Because of the potential for minimal weight addition to the vehicle, CF-TVC systems may be retrofitted to an existing aircraft's engine without significant structural alteration of the airframe. Similar benefits are expected for the design of new exhaust nozzle concepts for both aircraft and missile applications, namely a

reliable, robust system with a relatively low initial cost, and minimized maintenance costs.

## Facilities

The majority of measurements were conducted in the blow-down compressed air facility of the Fluid Mechanics Laboratory located at Florida State University. (The complementary studies at China Lake Naval Air Warfare Center will only be summarized here.) The facility is driven by a high-displacement reciprocating air compressor which is capable of supplying air at a maximum storage pressure of 160 bars. Large storage tanks provide a total capacity of 10 m<sup>3</sup> and are capable of driving the Mach 2 primary jet flow examined in this study continuously for up to 30 minutes. The supply air can also be heated by being passed through an array of resistive tank heaters having a maximum power output of 450 KW and capable of achieving stagnation temperatures in excess of 750 Kelvin. Visualization of the jets was achieved by creating laser sheet images of the vectored plane along the jet axis using frequency doubled Nd:YAG pulsed lasers. Fine condensation ice particles formed in the mixing region between the dry cold air of the primary jet and the moist ambient air scatter the laser light thus rendering the shear layers visible.

For the pitch-axis vectoring study, the blow-down facility was fitted with a rectangular nozzle having an exit aspect ratio of 4:1 (52 mm by 13 mm). The Mach 2 axisymmetric nozzle used for multiaxis thrust vectoring was designed to have the same minimum throat and exit plane cross-sectional area as the rectangular nozzle to ensure that, for the same stagnation pressure and temperature, the flow conditions for both jets were nominally the same. Contours of both nozzles were generated by a method of characteristics for a design Mach number of two and were run at their design pressure ratios. The jets were operated at stagnation temperatures between 300 K and approximately 700 K, corresponding to exit plane Reynolds numbers from 0.4 to 1.2 x 10<sup>6</sup>.

## Pitch Vector Control

To achieve thrust vector control, a secondary counterflowing stream needs to be established along the outer surface of one of the jet shear layers as shown previously in Figure 1a. This secondary stream is created by connecting a vacuum pump and manifold to a cavity placed along the periphery of the jet. To assure that the counterflowing stream acts along the appropriate shear layer of the jet, suction chambers must be created, the nature of which will depend on the nozzle geometry under consideration. This can be achieved quite easily in the rectangular geometry by the positioning of side plates attached to the ends of the collars, effectively isolating the secondary flow to either the upper or lower shear layer. Similar partitioning can be employed in axisymmetric jets to achieve multiaxis thrust vector control as will be discussed later.

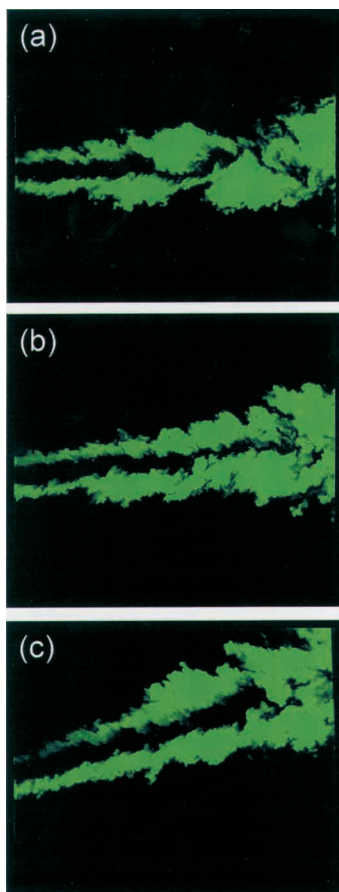


**Fig. 2 – Light scattering from the jet centerplane showing thrust vectoring at (a) 0°, (b) 6°, and (c) 16° using a collar geometry of  $G/H = 0.38$ ,  $L/H = 6.9$ , and  $R/H = 15.7$ .**

To demonstrate the CF-TVC concept for the pitch vectoring of a rectangular jet, a base study was conducted with flow visualization using planar laser scattering. The primary jet was unheated having a stagnation temperature of 300K, resulting in a low static temperature after expansion to Mach 2. Under these conditions, the entrainment of relatively moist air into the shear layer of the cold jet gives rise to ice crystal formation in the mixing region and thereby illuminates the jet shear layers during vectoring. The series of photographs in Figure 2 were taken over the streamwise distance of approximately  $7H$  to  $23H$ , and were captured by illuminating the jet with a 10-nsec exposure of the laser sheet positioned along the jet axis. When the vacuum system, connected to the upper collar, is deactivated and air is allowed to entrain freely into both the upper and lower shear layers, the jet exhausts along its geometrical axis as shown in Figure 2a. Under these conditions the collar arrangement operates analogously to a jet ejector configuration, albeit inefficiently due to the rapid divergence of the collar walls. When the vacuum system is activated creating secondary counterflow in the gap between the jet and the collar, thrust vectoring can be achieved as shown by the photographs in Figures 2b,c. The static pressure measured on the upper collar surface in the jet exit plane (essentially the secondary plenum pressure  $P_B$ ) was reduced from -0.061 bar in Figure 2b, to -0.29 bar in Figure 2c, corresponding to vector angles estimated from the photographs and corroborated using direct thrust measurements of 6° and 16°, respectively. The

jet could be vectored toward either the upper or lower collar by activating the appropriate vacuum system.

Due to the intense mixing which occurs in the shear layer of the vectored jet, it is not obvious whether the secondary flow drawn into the vacuum system originates primarily from ambient fluid or from the jet itself. To obtain a more complete physical understanding of the countercurrent flowfield in the vicinity of the collar, the mean velocity was captured using particle image velocimetry, a non-intrusive technique requiring that the primary and secondary streams be seeded with submicron particles and illuminated using a pulsed laser.<sup>2</sup> The mean velocity-vector field and corresponding isovelocity contours obtained for a Mach 2 jet vectored at  $\delta_v = 8^\circ$  are shown in Figure 3. A close examination of the velocity vectors reveals that the maximum countercurrent velocity occurs near the midpoint of the collar, at  $x/H \approx 4$  in Figure 3, and corresponds to nearly 30% of the primary jet velocity. These high secondary velocities are due to both the vacuum system as well as the natural entrainment characteristics of the primary jet. What is perhaps most interesting is that the majority of the counterflow is eventually entrained by the jet and carried downstream, resulting in relatively small amounts of secondary flow entering the vacuum system. The maximum amount of mass drawn into the secondary plenum is less than 2% of the primary jet mass flow rate.

Casting the experimental thrust performance data into a common format, which can be used for nozzle design, requires an examination of the parameters influencing jet curvature in the proximity of the collar surface. For purposes

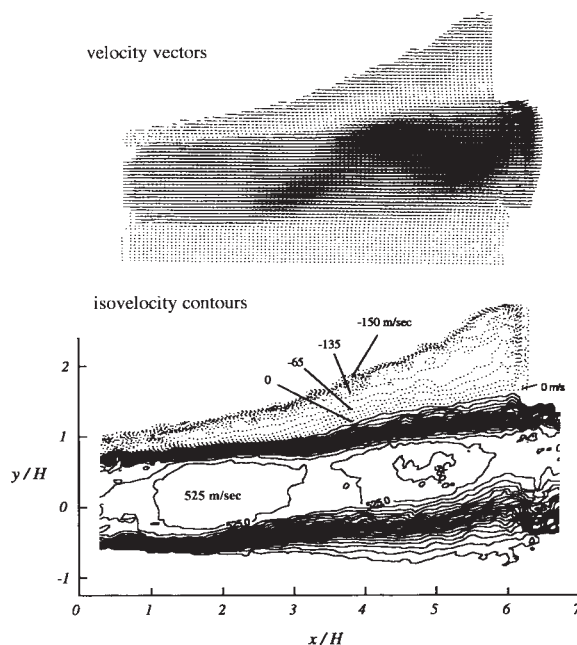


**Fig. 3 – Velocity vector field and isovelocity contours obtained using particle image velocimetry for a jet at Mach 2 for  $G/H = 0.38$ ,  $L/H = 6.9$  and  $R/H = 15.7$ .**



of discussion, we will consider the pitch vectoring of a rectangular jet as shown schematically in Figure 1a and visually in Figure 2, and subsequently extend the scaling to other nozzle geometries, in particular the axisymmetric nozzle. The exit vector angle,  $\delta_v$ , depends on the length of the collar surface,  $L$ , the forward momentum of the jet per unit depth,  $\rho_1 U_1^2 H$ , and the pressure distribution on the collar surface, where the subscript 1 indicates mean quantities in the jet exit plane. Experimental work<sup>1,2</sup> has shown that the pressure distribution on the collar surface is nominally uniform over the forward half of the collar where the majority of the side force is taken up, and may be proportionally controlled by varying the secondary plenum pressure  $P_B$ . The relationship between the plenum pressure and vector angle is required for nozzle design, and has been examined over a wide range of conditions for both subsonic<sup>2</sup> and supersonic<sup>3,5</sup> jets. (Note that the scaling arguments and experimental results presented here are relevant for jets operated near their design pressure ratios only.)

The two-dimensional momentum equation in cylindrical coordinates provides insight into the physical phenomena affecting the relationship between  $\delta_v$  with  $P_B$ . Recognizing that viscous terms are small compared to inertial effects in a free jet, and assuming that the flow is nominally parallel in the streamwise direction the momentum equation can be simplified to the expression given previously in Eqn. (1). To develop a scaling equation for CF-TVC performance, it is assumed that the jet uniformly arcs at a constant radius of curvature,  $R$ . This assumption is fairly accurate as long as  $R$  is significantly larger than the jet dimension  $H$ ; hence, the analysis applies to small vector angles.

Integrating from one side of the jet to the other, the right hand side of Eqn. (1) represents the streamwise momentum. Since streamwise momentum is conserved in a free jet flow, this quantity is equal to the momentum flow in the jet exit plane per unit depth,  $\rho_1 U_1^2 H$ . The integral on the left-hand side is known from the boundary conditions. On the radially outward shear layer, the pressure is equal to that of the ambient,  $P_\infty$ , on the inner shear layer, the pressure is approximately that of the secondary plenum  $P_B$ . Thus we obtain:

$$P_\infty - P_B = \frac{\rho_1 U_1^2 H}{R} \quad (2)$$

Upon reaching the streamwise extent of the collar,  $L$ , the counterflow ceases and with it the mechanism for sustaining the cross-jet pressure gradient. As a result, the jet exits straight into the atmosphere, at an angle  $\delta_v$ , as seen in Figure 1a. The jet curvature can be related to the exit vector angle and the length of the collar using the expression:

$$R = \frac{L}{\sin \delta_v} \quad (3)$$

Combining the last two expressions and solving for the vector angle in terms of the control pressure, we have:

$$\sin \delta_v = \frac{(P_\infty - P_B)L}{\rho_1 U_1^2 H} \quad (4)$$

Experimental observations of pitch vectoring in rectangular jets, for both subsonic and supersonic conditions show that this expression holds true, to a good approximation, over a wide range of flow conditions and collar parametrics as shown in Figure 4. The data presented in the figure include a variety of studies of supersonic flow at Mach 2, where nozzle gap  $G$ , collar length  $L$ , radius of curvature  $R$ , and jet stagnation temperature have been varied; thrust vector angles were determined using a six-component thrust stand and were corroborated with control volume analysis. The pitch vector data, indicated by the solid symbols enclosed within the hatched region, demonstrate a nearly linear relationship between normalized plenum pressure and jet response for primary stream stagnation pressures held fixed at the design pressure ratio for Mach 2. Under these conditions, weak shocks are present due to the asymmetric pressure distribution in the jet exit plane caused by underexpansion in the direction of secondary counterflow.

The scaling relationship observed in Figure 4 can be used to design nozzle-collar systems in other geometries by considering that the expression on the right hand side of Eqn. (4) is effectively the ratio of the side forces acting on the collar surface  $(P_\infty - P_B)A_{side}$  to the axial force imposed by the jet  $\rho_1 U_1^2 A_{jet}$ , where the ratio  $A_{side}/A_{jet}$  can be simplified to  $L/H$  for the rectangular geometry. Hence, the basic scaling law we want to consider for more complicated geometries is given

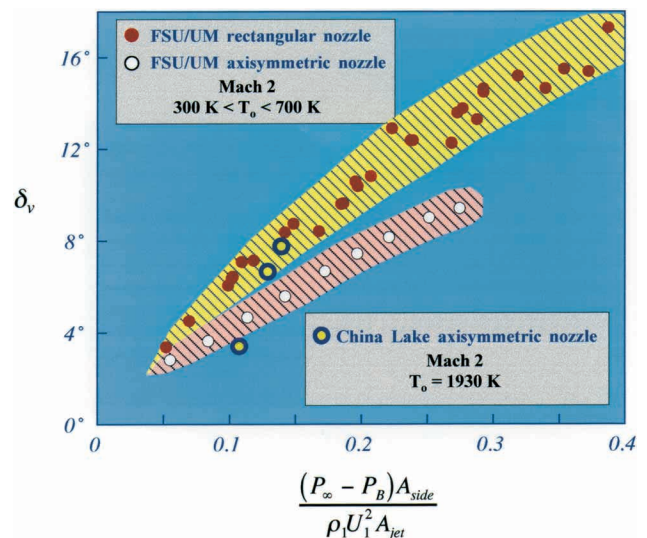


Fig. 4 – Counterflow thrust vectoring performance at Mach 2 for rectangular and axisymmetric nozzles.



by Eqn. (5), valid for nozzles operated near their design pressure ratios.

$$\delta_v = fcn \left\{ \frac{(P_\infty - P_B)A_{side}}{\rho_1 U_1^2 A_{jet}} \right\} \quad (5)$$

## Multiaxis Thrust Vector Control

Extending the CF-TVC concept from pitch vectoring to multiaxis operation requires a collar design which effectively directs counterflow along the jet shear layer. Since the vacuum source alone cannot direct the flow, the collar must be partitioned to created chambers through which the secondary flow can pass and thereby establish a countercurrent shear layer. Figure 5 indicates the partitioning strategy employed for multiaxis vector control of an axisymmetric Mach 2 nozzle. When the vacuum source is connected to a particular chamber, a secondary counterflow is developed — bounded by the collar surface and a segment of the jet shear layer. This, in principle, causes the primary jet to vector in a direction normal to the shear layer along which counterflow is established. A single vacuum source was connected to the chambers via control valves allowing independent vectoring in any of the six directions as desired.

Instantaneous planar laser scattering images showing the cross-sectional view of the unvectored and vectored axisymmetric jet at  $x/D \approx 2.5$  are shown in Figure 6; note that the camera is positioned off-axis to avoid interaction with the high-speed jet, creating the observed oblique view. A close examination of the images reveals that not only does

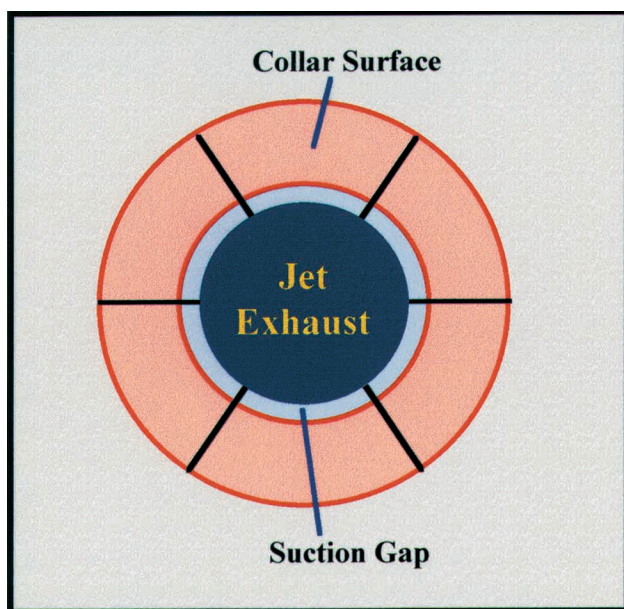


Fig. 5 – Schematic of the end view of the axisymmetric CF-TVC nozzle showing six-sector partitioning.

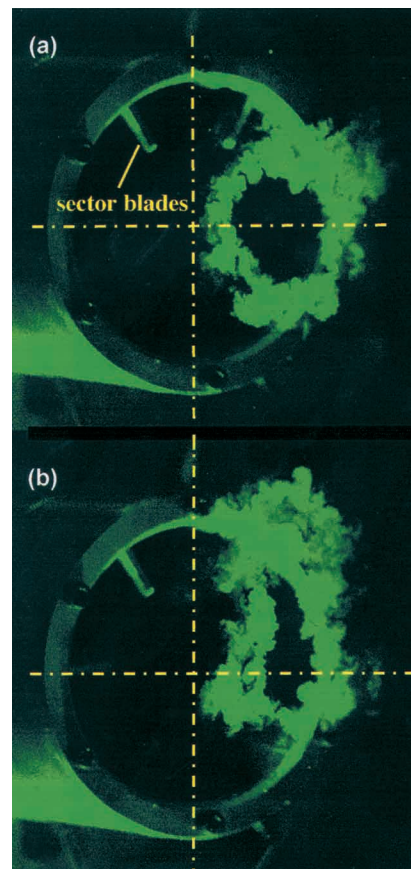



Fig. 6 – Planar laser scattering images of a Mach 2 axisymmetric jet cross section at  $x/D \approx 2.5$  for (a) unvectored jet and (b) jet vectored into uppermost sector at  $\delta_v = 10^\circ$ .

the jet move toward the chamber with counterflow, but the jet shape is altered considerably. We believe this is primarily due to the difference in the mixing rates of the countercurrent shear layer (upper shear layer in Figure 6b) and the shear layer regions isolated from secondary counterflow. For instance, if we compare the top portion of the jet shear layer in Figure 6b with the lower portion, it is apparent that the upper layer has diffused over a significantly larger area. This observations may allow the CF-TVC concept to be used not only for vector control but for mixing enhancement as well, which may be desirable for reducing jet noise or thermal signature. The crosshairs provide a frame of reference to compare the unvectored and vectored flow. There is a slight vertical shift in the lower shear layer, but the upper layer is considerably displaced. Thrust stand measurements indicate that the effective jet deflection is  $\sim 10^\circ$ , which is difficult to detect in the oblique view of Figure 6 due to the relatively small streamwise distance where the images were captured.

A summary of the axisymmetric jet vectoring as a function of the static pressure parameter is provided in Figure 4 to allow comparison to the pitch vectoring data; multiaxis thrust vector data are shown for studies conducted at Florida State University/University of Minnesota and China Lake. Although the axisymmetric nozzle data show reasonably linear behavior, the pitch vectoring results obtained using the rectangular nozzle appear to be slightly more efficient, namely larger vector angles can be achieved with lower vacuum pressures developed in the secondary plenum. We



believe the primary reason for these differences is due to leakage between adjacent chambers of the collar assemblies for the axisymmetric arrangement. This was determined by monitoring the static pressure distributions in the chambers adjacent to the primary chamber where vacuum is applied. These measurements indicated that counterflow is not completely isolated from other parts of the shear layer, resulting in a degradation of performance due to the transverse pressure gradient across the shear layer. It is also difficult to determine the appropriate side area  $A_{\text{side}}$  which is used to develop the scaling in Figure 4; a simple projection of the active sector was used when plotting the data. The maximum vector angle of  $10^\circ$  achieved for the axisymmetric study compared to nearly  $20^\circ$  for the rectangular jet, is not due to an inherent limitation of the concept, but rather caused by the smaller side area of the axisymmetric collar compared to the rectangular collar when acted upon by the same available vacuum pressure ( $P_\infty - P_B$ ). Although these three-dimensional effects will undoubtedly influence the collar performance, we believe that they can be minimized by improvements in collar design.

## Performance Considerations

Performance of the multiaxis CF-TVC system was also documented in terms of secondary mass flow rate, jet dynamic response and hysteretic behavior. The mass flow drawn through the secondary vacuum system was determined to be consistently less than 2% of the primary jet mass for the unheated primary flow (stagnation temperature of 300 K), and significantly lower when the primary jet was heated. In the FSU/UM experiments described above, the primary mass flow rate was between approximately 0.5 and 0.75 kg/sec, for hot and cold jet conditions respectively. The secondary mass flow rate was below 0.015 kg/sec for all conditions examined. Dynamic performance of the multiaxis system was also evaluated for the axisymmetric configuration. A solenoid valve was used to activate and deactivate counterflow to a desired chamber and two different measurements were used to determine the dynamic response of the jet. In the first approach, the planar laser scattering images were recorded on video during this transient process and a time stamp was superimposed on this record. The video record shows the jet being deflected from  $\delta_v = 0^\circ$  to  $9^\circ$  and vice versa in significantly less than a tenth of a second, the lowest subdivision on the time stamp. This places a lower limit of 90 degrees/sec on the jet deflection rate. A second method was then used to determine the jet dynamic response more precisely. The unsteady plenum pressure  $P_B$  on the collar surface was monitored using a fast response pressure transducer (minimum flat frequency response of 40 kHz) while counterflow was cycled on and off. These measurements indicate that the jet could be deflected from zero to 9 degrees in less than 50 ms, resulting in jet vectoring rates of at least 180 degrees/sec.

Due to the entrainment differential, a small degree of jet

turning is possible, in principle, without a collar surface, however it is the addition of an extended collar surface of length  $L$  that makes CF-TVC a viable technology. First, it channels the secondary flow in parallel with the primary flow, effectively inducing a countercurrent mixing layer over a finite extent of the jet column. Second, it restricts the natural entrainment of the jet, intensifying the cross-stream pressure gradient. Finally, it gives the pressure forces a surface over which to act. A longer collar has more surface area for the pressure forces to act on thus a smaller pressure differential will impart an equal transverse force on the nozzle-collar assembly. In other words, with a longer collar, the same vector angle is achievable with a smaller amount of vacuum from the secondary flow system. The net effect is a reduction in pumping power losses.

While the collar is vital to the efficiency of the CF-TVC system, it poses a potential problem that can disrupt the continuity of the operating curve. This condition, a result of the bistable interaction between a free jet and a wall, is one in which the jet attaches to, and reaches a stable equilibrium on, the wall. It has been observed, under certain operating conditions by previous CF-TVC investigators,<sup>1,2</sup> that the jet attaches to the collar surface during vectoring. This is unacceptable from a design standpoint as, in a flight situation, this may cause a loss of control. Furthermore, to release the jet from the collar, the differential control pressure must be reduced beyond that which was required to cause attachment. This hysteretic behavior makes a continuous vector-control system very difficult (if not impossible) to implement. Fortunately, this situation can be prevented in many instances by correctly tailoring the geometry of the collar.<sup>6</sup>

The important thing to bear in mind when designing a CF-TVC system is that wall attachment can only occur if an equilibrium can be sustained as shown in Figure 1b. This means that the entrainment mechanisms within the jet must be able to sustain the low pressure necessary to hold the jet attached to the wall. The shorter the collar, the sharper the jet must turn in order to attach; thus a lower plenum pressure will be required. Furthermore, with a short collar, the shear layer has less contact with the secondary stream, making it more difficult for the pumping mechanism within the jet to generate the low pressure required to hold itself to the wall. Consequently, if the collar is sufficiently short, attachment will not occur.

There is a unique equilibrium location where the attaching streamline intersects the collar. This location depends on the gap width, the mixing dynamics of the shear layer, and the amount of secondary flow leaving (or entering) the recirculation zone. A large gap places the collar surface farther away from the jet, resulting in a longer attachment length. Enhanced shear layer growth rates mean the jet is more effective in sustaining low pressures along the collar surface. Likewise, counterflow being drawn from this region by a



secondary pump assists the jet in sustaining the low pressure necessary to hold itself to the wall. These two latter conditions enable the jet to turn with a smaller radius of curvature, resulting in a shorter attachment length. If the collar is longer than this equilibrium attachment length,  $L_{att}$ , the jet will merely attach at the designated location, and follow the contour of the wall until boundary layer separation occurs. However, if the collar length is shorter than the equilibrium attachment length, i.e.  $L < L_{att}$ , the jet will not attach to the wall. When designing a collar, it is important to be able to estimate the attachment length based on the intended operating conditions. Ultimately, designing a CF-TVC system for aircraft or missile propulsion requires that a collar geometry be found which is capable of achieving the required thrust vector angle,  $\delta_v$ , while minimizing external drag, secondary mass flow pumping demands, and provide attachment-free operation over the entire operating domain of the vehicle.

## Flight Effects

The generally favorable characteristics of CF-TVC performance as described above are encouraging, however successful system integration of the concept requires at a minimum that the technology can be implemented during actual flight conditions. To examine this aspect of performance, the influence of a coflowing external stream was imposed on a rectangular jet (aspect ratio of 4:1) operated at a Mach number of 1.4; external coflow Mach numbers were examined between 0.3 and 0.7. A schematic of the CF-TVC system and coflow hardware is shown in Figure 7. The coflow was established by placing a rectangular duct around, and extending downstream of the nozzle-collar hardware. The duct was equipped with glass windows to allow optical access for flow visualization; surface pressures were used together with momentum flux measurements to evaluate the effective thrust vector angle using a control volume analysis.

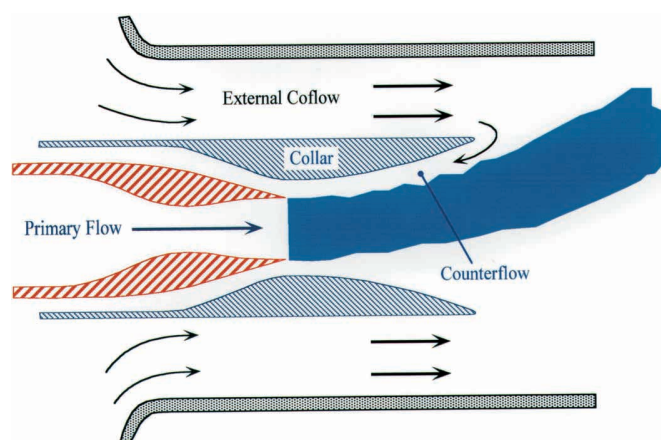


Fig. 7 – Side view of a Mach 1.4 rectangular jet positioned in a coflow duct to simulate forward flight effects.

A summary of the CF-TVC performance of a rectangular jet for various counterflow and external coflow levels is provided in Figure 8 together with the pitch vector control presented in Figure 4 for comparison. Again  $P_B$  represents the secondary plenum pressure measured on the collar surface in the jet exit plane. At first glance it appears that thrust vector performance with external coflow is very similar to the behavior without coflow, in that the jet vector angle increases nearly linearly with increasing vacuum pressure. However, a closer examination reveals that, albeit small, there is a systematic degradation in the performance with coflow. For a given differential pressure across the collar, the jet response indicated by  $\delta_v$  decreases as the coflow Mach number increases. This effect can be understood if we consider the effect of vectoring in one direction, for instance up, on the flow regime on the opposite side, in this case the region below the curved primary jet. In the configuration used in our experiments, when counterflow is actuated in the upper shear layer, there is no flow through the lower gap between the jet and lower collar. But the lower shear layer of the primary jet and the upper shear layer of the lower coflowing stream both entrain fluid from the region bounded by these two shear layers creating a low pressure zone — essentially a wake — on the lower side of the primary jet. This in turn reduces the side force on the nozzle-collar assembly and the effective angle  $\delta_v$ . As the entrainment rate increases due to increased coflow Mach number, so does the wake effect and the detrimental influence on performance. However, at higher thrust vector angles the pumping action of the primary jet has a reduced impact on the surface pressures of the lower collar for a fixed coflow Mach number. Hence, as  $\delta_v$  increases the difference between coflow and no-coflow experiments should diminish, which is the trend seen in Figure 8.

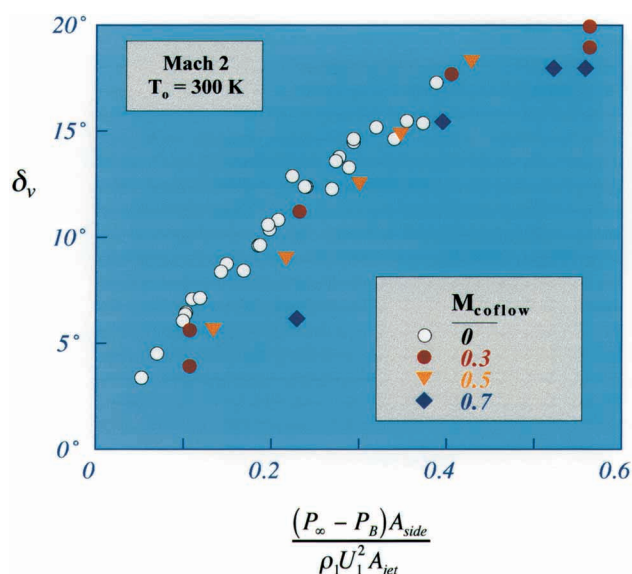



Fig. 8 – Thrust vector performance of a rectangular jet operated in the presence of an external coflowing stream.





The degradation in CF-TVC performance can be alleviated, in principle, if atmospheric pressure is maintained in the regions not actively experiencing counterflow. This could be achieved by ducting some of the freestream flow into the inactive secondary plenum, and thereby “filling” this region to reduce the wake effect. Although the actual hardware used to accomplish this will depend on the overall vehicle configuration, we believe that the effect of coflow on CF-TVC performance can be implemented using this approach.

### Closing Remarks

We have provided a brief overview of the issues which must be considered in the design of a thrust vector system based on counterflow. It has been shown that through CF-TVC it is possible to vector thrust in multiaxes in a continuous fashion using a fluidic approach. The performance of the nozzle system is relatively insensitive to jet stagnation temperature, at least over the range studied to date (300 to 1930 K), and the thrust vector angle is approximately a linear function of the static pressure developed in the counterflowing stream. Although many issues need to be examined further, such as the presence of shock waves within the collar region for jets operated off-design, and further study at high temperatures, the inherent simplicity of this method makes it a promising concept for vectoring thrust.

### Acknowledgments

The authors would like to thank the Office of Naval Research for support of this work and the guidance we have received from technical monitor Dr. Gabriel Roy. We would also like to acknowledge our colleagues Professor F. Alvi, D. Forliti, G. Schmid, and M. Van der Veer.

### References

1. Van der Veer, M.R. and Strykowski, P.J., “Counterflow thrust vector control of subsonic jets: continuous and bistable regimes,” *J. Prop. & Power*, Vol. 13, No. 3, 1997, pp. 412-420.
2. Strykowski, P.J., Krothapalli, A. and Forliti, D.J., “Counterflow thrust vectoring of supersonic jets,” *AIAA J.*, Vol. 34, No. 11, 1996, p. 2306-2314.
3. Young, T., “Outlines of experiments and inquiries respecting sound and light,” Lecture to the Royal Society, Jan. 1800; also *Journal of the Royal Aeronautical Society*, Vol. 61, 1957, p. 157.
4. Strykowski, P.J., Krothapalli, A. and Jendoubi, S., “The effect of counterflow on the development of compressible shear layers,” *J. Fluid Mech.*, Vol. 308, Feb. 1996, p. 63-96.
5. Washington, D.M., Alvi, F.S., Strykowski, P.J. & Krothapalli, A., “Multiaxis fluidic thrust vector control of a supersonic jet using counterflow,” *AIAA J.*, Vol. 34, No. 8, 1996, p. 1734-1736.
6. Schmid, G.F., “Design and optimization of a counterflow thrust vectoring system,” M.S. Thesis, University of Minnesota, Minneapolis, June 1996.

# Runway *Models*

Designing gas turbines has long depended on a lot of empirical work—“cut and try,” in engineers’ parlance. But now we’re reaching a point in computational power and modeling sophistication where that may all change.

Advances in computational fluid dynamics and related areas of computational combustion mechanics are revolutionizing the field of gas turbine design. Engineers have successfully demonstrated simple models—semi-analytical mechanistic models—for various combustors. They are now ready to validate advanced models for combustion design.

Hukam Mongia describes how the state of aero-thermal design has advanced over the last quarter century, and what we can expect for the future as engineers continue to push the frontiers of combustion modeling. *-J.P.*



---

# Aero-Thermal Design Methodology for Gas Turbine Combustion Systems: Future Direction

---

**Hukam C. Mongia\***

*Combustion Center of Excellence  
GE Aircraft Engines, Cincinnati, Ohio*

---

GE Aircraft Engines (GEAE) has introduced several new aeropropulsion gas turbine engines with improved combustion systems since 1994 including the CFM56 dual annular combustor (DAC), the CF6-80 low-emissions single annular combustor (LEC), the GE90 DACII, in addition to the dry low emissions (DLE) for the LM1600, LM2500 and the LM6000. Development and validation of advanced turbulence and radiation models as part of the National Combustor Code (NCC), is now pursued in collaboration with NASA. These activities pave the way for combustion design process that will use computational combustion dynamics-based methods unlike the most conventional “cut-and-try” design practice.

## Introduction

The empirical/analytical gas turbine combustor design methodology has progressively improved over the last 25 years in regard to: a) the design process, b) the aero-thermal combustion models, and c) simulations including accurate representation of the combustion geometry, numerics and other critical steps. Since 1986, General Electric (GE) has developed two techniques (namely, hybrid modeling and anchoring methodology) for getting quantitatively good agreement with gas turbine combustor data in regard to combustion efficiency, HC, CO, NO, lean blowout, burner exit temperature profile, pattern factor, and liner wall temperatures.

The empirical/analytical combustion design methodology has been used in the designs of numerous combustors<sup>1,2</sup>.

Simple models, termed as semi-analytical mechanistic models (SAM), have been formulated and their feasibility demonstrated for both the diffusion-flame and premix combustors<sup>3,4</sup>. Anchored Computational Combustion Dynamics (CCD) based approach introduced in 1996, that has become a standard practice in the combustion design procedure<sup>5</sup>. With recent advances in grid generation, computational speed, and combustion models, validation of advanced models as the next logical step of combustion design tools evolution, has been started.

## Advanced Combustion Code

Having established Generation 1 SAM and anchored CCD methodology, several activities have been initiated recently to bench mark and/or improve:

- a) CFD capability of the design code
- b) Baseline turbulent combustion models based on eddy-breakup (EDC) and scalar transport PDF
- c) Turbulence models relevant to gas turbine combustion
- d) Radiation model
- e) Spray model
- f) Laminar flamelet modeling with reduced and skeletal mechanisms
- g) Large eddy simulation (LES).

The following paragraphs give brief description of the activities in each of these eight areas.

An Advanced Combustion Code (ACC) is currently being developed to further advance the use of Computational Combustion Dynamics (CCD). ACC has complex geometry representation capability via unstructured single block grids,

---

\*Copyright 1998 by the author. Published by ONR with permission.



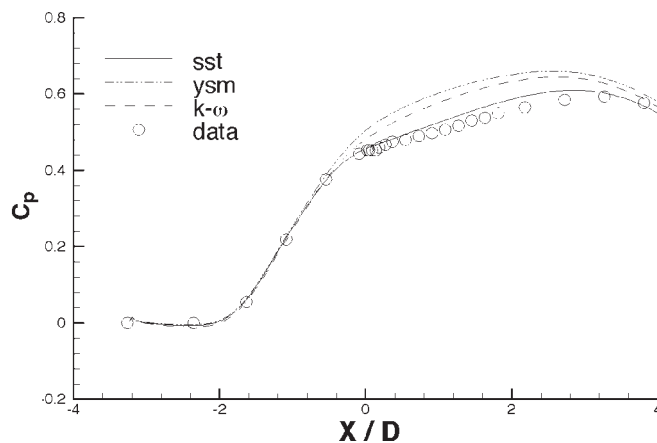


Fig. 1 – Comparison between predicted (by Nikjoo and Mongia, 1999) and measured (by Driver, 1991)  $C_p$  distribution.

and comprises of a number of advanced combustion/spray/turbulence models that are being developed in a modularized fashion. The ACC solver is based on a fully implicit pressure correction algorithm with co-located grids. An overview of an early version of ACC is given by Tolpadi *et al.*<sup>6</sup> This code allows a more accurate representation of staged combustion systems including DLE.

Since the first use of CCD in combustion design<sup>1</sup>, the need to improving turbulence models for gas turbine combustion was emphasized. In spite of concerted effort by several turbulence modeling groups over the last 25 years, the predictive accuracy for turbulent combustion field has not improved. Even after having expended a considerable effort on carefully measuring and modeling isolated sub-component flow-fields relevant to gas turbine combustors, it was not possible to improve accuracy of turbulent combustion models. For example, refer to the numerical calculations of the jet diffusion flame performed by Tolpadi *et al.*<sup>6</sup> using the eddy breakup, eddy dissipation and the scalar PDF transport combustion models with the standard k- $\epsilon$  model. Even though one can offer several good reasons for the failure of the models to achieve acceptable level of quantitative agreement for such a simple test case, it is nevertheless a discouraging state of the turbulent combustion modeling.

Encouraged by recent advances in turbulence modeling<sup>7-9</sup>, this author's group recently started to reassess the strategy for improving turbulence modeling for the following three areas of interest in gas turbine combustors.

There is an urgent need to predict accurately the pressure recovery and total pressure loss distribution in gas turbine combustor diffusion system so that the designer can calculate the distribution of airflow, static and total pressure distribution around the combustor dome and inner and outer liners. Karki *et al.*<sup>10</sup> demonstrated that 3-D diffusion system calculations can be done if a) one had an accurate turbulence model for flows involving adverse pressure gradients; and b)

sufficiently fine grids were used for simulating production gas turbine combustor diffusion system.

Nikjoo and Mongia<sup>11</sup> recently evaluated the performance of the standard k- $\epsilon$  model, a nonlinear Yang and Shih k- $\epsilon$  model (YSM), k- $\omega$  model (high and low-Reynolds number formulation), and shear stress transport (SST) model for well-defined experimental data for adverse pressure gradients (involving separated boundary layer) documented by Driver<sup>12</sup>. Fine-grid calculations were done for the region between the first measuring station at  $x/R_0 = -6.531$ , and the exit plane at  $x/R_0 = 11.4$  where  $R_0 = 70\text{mm}$  is the cylinder radius and the boundary layer separation takes place at  $X = 0.0$ .

Figure 1 shows comparison between the measured  $C_p$  and predicted  $C_p$  by the standard k- $\epsilon$  model, YSM, a nonlinear k- $\epsilon$  model, the low-Reynolds k- $\omega$  model, and SST model. It shows that a significantly improved  $C_p$  correlation is achieved by the SST model. All the models predicted similar  $C_p$  in the first half of the flow in the region with adverse pressure gradient. However in the recovery region, the performance of the k- $\omega$  and YSM models are not satisfactory. The SST model's predictions are in very good agreement with data in both the front and recovery regions.

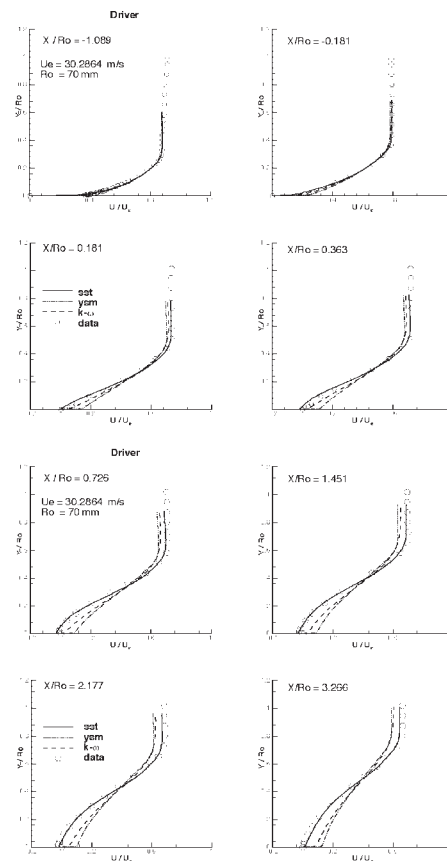


Fig. 2 – Comparison between predicted (by Nikjoo and Mongia, 1999) and measured (by Driver, 1991) axial velocity profiles in a separating boundary layer.

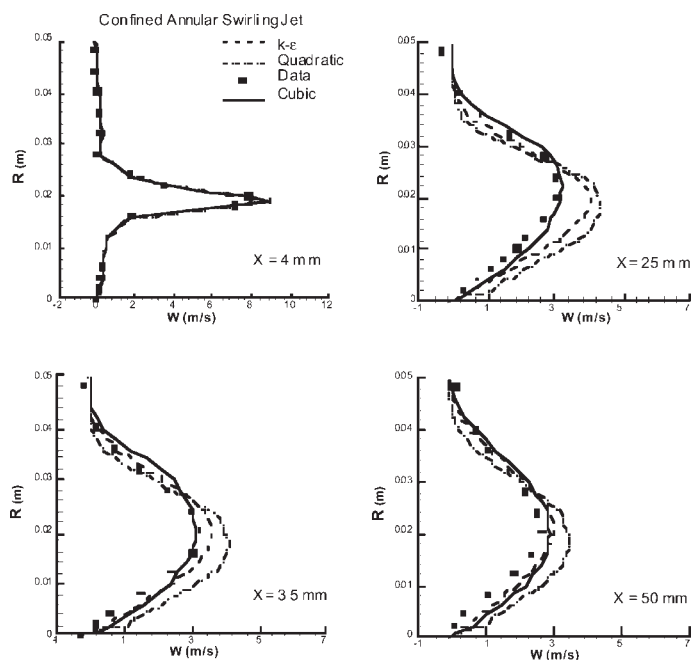


Fig. 3 – Comparison between predicted (by Nikjoo and Mongia, 1998) and measured (by Nikjooy et al., 1993 ) swirl velocity profiles of a confined annular jet a

In other words, when the eddy viscosity is properly corrected for the adverse pressure gradients (as done in the SST model), it is possible to correctly predict  $C_p$  distribution in a diffusion system, a pre-requisite for claiming to have an acceptable diffusion system model.

Comparisons of the measured and predicted mean axial velocity component by the SST,  $k-\omega$  model, and YSM model are shown in Figure 2 for different axial stations. The axial velocity component calculated by the SST model closely resembles the experimental data. There are substantial differences between the measured profiles and the predictions with the  $k-\omega$  and YSM models. The YSM and the  $k-\omega$  models failed to predict the velocity profiles correctly in the separation zone,  $X \geq 0$ . The mean axial velocity profiles predicted by the SST model are in good agreement with experiment both in the inner and outer flow regions. In the downstream stations, the results of YSM and  $k-\omega$  models are almost similar but they are significantly different than the measurement.

Co-annular sub- and super-critical swirling flows are routinely used in gas turbine combustors. The standard  $k-\epsilon$  model fails to capture critical features of these flows. Nikjoo and Mongia<sup>13</sup> have recently evaluated the performance of the standard  $k-\epsilon$  model, quadratic and cubic YS models for the two sets of swirling flows, namely, a single swirling jet with no sudden expansion, and a co-annular confined swirling jet. Comparisons of the measured and predicted mean swirl velocity and profiles shown in Figure 3 co-annular jets.

As expected, the standard  $k-\epsilon$  model captures qualitatively

the flow field characteristics. But there are substantial differences in regard to swirl velocity (which model over-predicts). Similar discrepancies are noted in axial velocity, as well.

The performance of the quadratic nonlinear  $k-\epsilon$  model is essentially comparable with that of the standard  $k-\epsilon$  model.

However, the cubic non-linear  $k-\epsilon$  model does significantly better in regard to simultaneously matching swirl velocity profile, jet spreading rate (i.e., location of the peak) and the peak value of the axial velocity. The major deficiency of this model is the under-prediction of the jet centerline velocity. More modeling work is planned to get better agreement with the data.

In order to meet the combustion system life requirements within the constraints of significantly reduced cooling air availability, designers are being challenged to reduce the structure temperature margin used in the past applications.

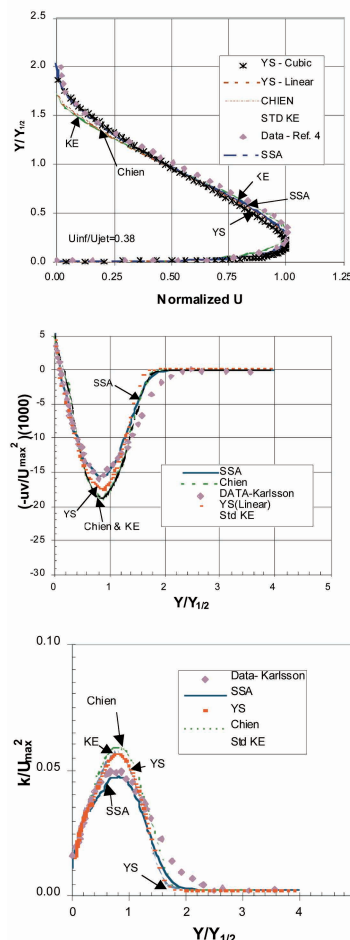


Fig. 4 – Radial profiles of mean axial velocity, shear stress and turbulence KE of a turbulent wall jet. a) Heat transfer coefficient along jet center line. b) Radial profiles of heat transfer coefficient at  $X/D = 3.0$ . c) Radial profile of heat transfer coefficient at  $X/D = 10$ .

This means a more optimized utilization of the available cooling air and significantly improved prediction capability. Work is therefore needed to improve both the radiation and convective heat transfer models similar to what is described in the following paragraphs.

A non-gray sum-weighted, narrow-band radiation model consistent with finite-volume 3-D gas turbine combustion model has been formulated and coded for incorporation as a module to the National Combustion Code being developed jointly by NASA and industry. Kumar *et al.*<sup>13</sup> have done preliminary assessment of this model. The wall temperature levels calculated by the wide band model (which is computationally faster than the narrow-band model by a factor of more than 5) are quite close to those of the narrow-band model for a typical liner at 40 atm. and 0.03 fuel/air ratio; the resulting root-mean-square (RMS) error is quite small. On the other hand, the differences between the narrow-band and the conventional state-of-the-art models are substantial. For nonluminous flames requiring no estimates for soot concentration, a quasi-3D anchored reduction model<sup>14</sup> is about as good as one needs for calculating temperature levels of typical combustor structure.

The formulation and validation of a CFD-based convective heat transfer model is being done in three steps. Step one involves the validation of the model with benchmark quality data in regard to flow field, film effectiveness and heat transfer coefficients. Several promising turbulence models have been evaluated.<sup>15</sup> Figure 4 shows typical comparison between predicted and measured data for turbulent wall jet in regard to mean axial velocity, shear stress and turbulence kinetic energy. Clearly, So and Sarkar turbulence model (SSA) is superior to other turbulence models (Figure 4) including standard k- $\epsilon$ , and models proposed by Chien, and Yang and Shih (YS). Work is in progress for Step 2 that involves making film effectiveness predictions for typical gas turbine combustors, followed by (in Step 3) validation with measured temperature levels and gradients of combustor dome and liners.

Convective heat transfer model validation for multi-hole liners (also called effusion cooling) is similarly being conducted in the three steps as explained above for the nugget liners. Kumar and Mongia<sup>16</sup> compare their predictions with data from Sen<sup>17</sup>, and Sinha<sup>18</sup> for a single row of inclined jets to a well-defined cross-flow stream. Typical comparison for heat transfer coefficient (Figure 5) and film effectiveness (Figure 6) with the SSA, YS and the standard k- $\epsilon$  models clearly show preference for the SSA model for near-wall heat transfer and fluid flow calculations.

Numerical calculations of a jet diffusion flame were performed by Tolpadi *et al.*<sup>19</sup> using the eddy breakup, eddy dissipation and the scalar PDF transport combustion models with the standard k- $\epsilon$  model. The agreement between data and calculations was rather unacceptable. Even though one

can offer several good reasons for the failure of the models to achieve acceptable level of quantitative agreement for such a simple test case, it is nevertheless a discouraging state of the turbulent combustion modeling.

Even though a variety of the two-step eddy break-up model first used by Reynolds *et al.* (1977) are being used in industry, no one is quite happy with its demonstrated accuracy levels. Hura *et al.*<sup>20</sup> have expended considerable effort in establishing how far one can go in anchoring a two-step eddy breakup model in regard to matching a single cup flow field data from the LM6000 DLE mixer. As shown in Figure 7, one can indeed get a good anchored agreement with measured centerline axial velocity using standard k- and 2-step eddy breakup models.

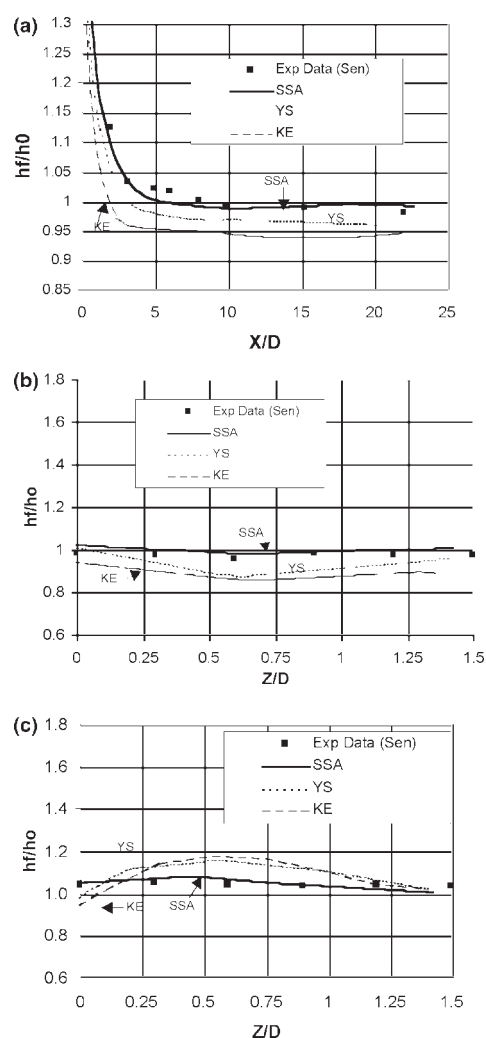


Fig. 5 – Comparison between measured (by Sen, 1995) and calculated heat transfer coefficient (by Kumar and Mongia, 2000) for a single 35-degree inclined jet in cross-flow. a) Film effectiveness along the jet centerline. b) Radial profiles of film effectiveness at  $X/D = 1.0$ . c) Radial profiles of film effectiveness at  $X/D = 15$ .



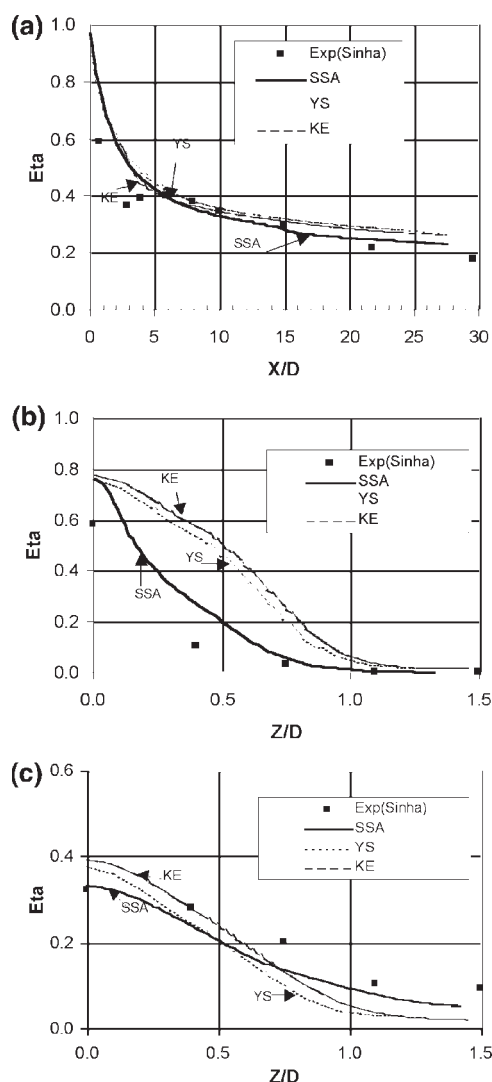


Fig. 6 – Comparison between measured (by Sen et al., 1991) and calculated film effectiveness (by Kumar and Mongia, 2000) for a single 35-degree inclined jet in cross-flow.

It is logical that a skeletal mechanism is needed for accurately predicting HC, CO and NO<sub>x</sub> emissions. One had to split up this in two steps – flow field calculations with simpler turbulence/chemistry interaction model (e.g., a 2-step eddy breakup model), followed by a reactor network with a skeletal mechanism. Now it is possible to formulate a single-step approach. As an example, a laminar flamelet model has been used by Held and Mongia<sup>21</sup> to demonstrate its feasibility for predicting the flow-field, NO<sub>x</sub> and CO emissions levels of the LM6000 DLE mixer. Figure 8 demonstrates the NO<sub>x</sub> prediction.

Under partial sponsorship of the AFOSR Focused Research Initiative, Menon and his associates have been working on the use of large eddy simulation with linear eddy (LESLE) subgrid modeling. The feasibility of this approach for the LM6000 DLE mixer has recently been demonstrated<sup>22, 23</sup>. They used the same inlet profiles as anchored by Hura *et*

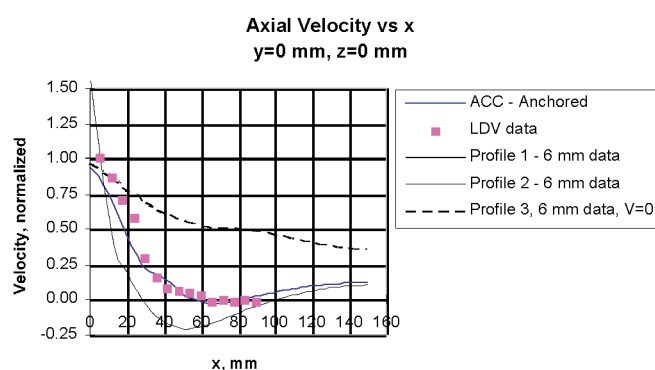


Fig. 7 – Comparison between measured and “anchored” centerline and corner axial velocity component of the LM6000 DLE mixer with a two-step eddy breakup model (from Hura et al., 1998).

*al.*<sup>20</sup> (Their predicted centerline axial velocity (Figure 9) should be compared with the results of Hura *et al.*, shown in Figures 7). This is a significant step forward with LESLE, considering that the first set of calculations were made by Kim and Menon<sup>22</sup> with no prior experimental values, and no attempt has been made to “further tune”. In subsequent calculations, Kim and Menon<sup>23</sup> have made further improvements to the models and obtained better agreement with data as shown in Figure 9. One of the significant advantages of the LESLE’s calculations is that it provides dynamic structure of the flame. This type of information along with measured data gives the research tools for providing the insight required to develop the technology in a more cost-effective and timely manner.

Combustion dynamic data from DLE combustor (premixed combustion) and CFM family (diffusion combustion) were collected and used to validate the Advanced Combustion Dynamics (ACD) model. Figure 10 illustrates the comparison of predicted and measured organ tone frequencies. Two discrete frequencies, namely mode 1 and mode 2 organ tones, have been observed in some CFM engines. The hollow triangles are the measured frequencies of mode-1 organ tone, while the hollow circles represent the mode-2 frequencies.

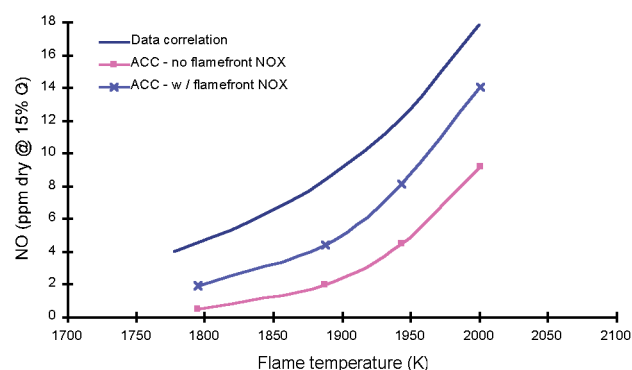


Fig. 8 – Feasibility demonstration of NO<sub>x</sub> prediction with a laminar flamelet model and comparison with data of the LM6000 DLE mixer (from Held and Mongia (1998)).

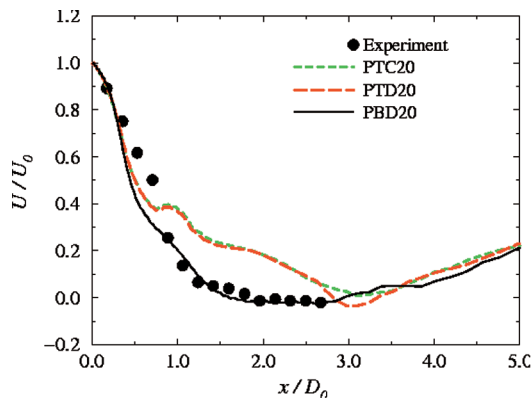


Fig. 9 – Comparison between measured and “anchored” centerline and corner axial velocity component of the LM6000 DLE mixer with Large Eddy Simulation (from Kim and Menon, 1999).

Since mean flow properties of combustor are required as inputs for the ACD model, the steady state CFD analysis with given cycle conditions were first conducted. Several variables, including temperature, velocity vectors, and steady state heat release, were extracted from steady state CFD flow field data and piped into a common interface of ACD model. The resonant frequencies were then obtained from the power spectrum density generated by the model. The predicted frequencies are presented by the solid symbols. The results from ACD model predict the increase in resonant frequency with increasing fan speed, the identical trend as observed from the engine data.

The current production DLE combustor is a triple annular premixed design. Two discrete frequencies, one at 450 Hz and the other from 600 to 650 Hz have always been observed in high power operating mode. Figure 11 shows the comparison between measured and predicted dynamic response. The predicted response (shown by the thin line in figure) is compared with a line drawn through the individual peaks of the measured spectrum plot (shown by the thick line in figure). The predicted value is obtained by taking the maximum of the individual responses from each ring,

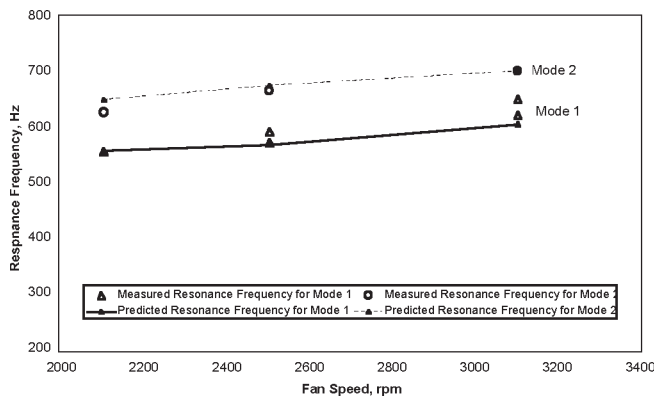


Fig. 10 – Comparison between predicted and measured organ tone frequencies for a diffusion flame combustor.

spectrum (b)-(e). The response characteristics of three different acoustic modes (plane wave,  $m=1$ , and  $m=2$ ), are plotted in solid, dotted, and dashed lines, respectively, in these figures. Within the frequency range of interest, the model predicts two dominant frequencies, one at 500 Hz and the other at 600 Hz. These frequencies are reasonably close to those observed from engine tests at the specified operating condition. It is self-illustrated from these figures that the 500 Hz mode is more active compared to the 600 Hz dynamics. Based on the current analysis, the dynamic pressures response in the vicinity of 500 Hz is mainly contributed by the plane waves ( $m=0$ ) from the middle and inner domes. The 600 Hz acoustic mode is a result of the first order circumferential mode arising in the outer ring. This analysis did not indicate the presence of a second-order mode in the combustor. In the high frequency region (above 1000 Hz) the current model over predicts the dynamic response. It is probably due to the effect of neglecting viscous effects in the governing equations.

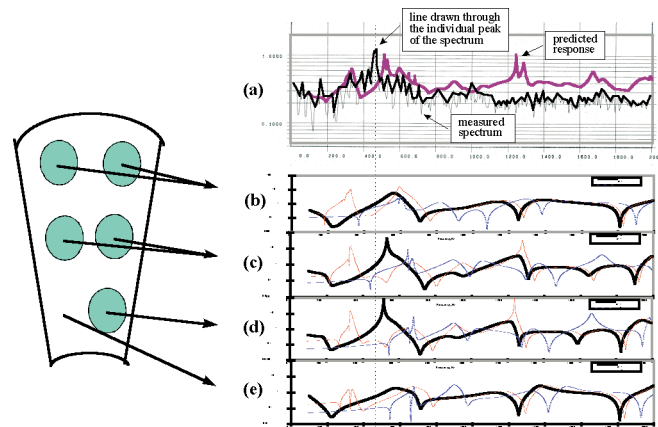


Fig. 11 – Comparison between predicted and measured power spectrum density plot for a premixed combustion system.

## Summary

The R&D effort has resulted in significant progress in the development and application of empirical/analytical design methodology that is used routinely in the design process, and in the semi-analytical mechanistic models formulation of their feasibility demonstration for both the diffusion-flame and premix combustors, further the feasibility and validation of anchored CCD methodology is well established and its use in the combustion design procedure is now a standard practice in CCoE.

Good progress has been made for validating the Advanced Combustion Code (w/ more accurate combustion models) with benchmark quality database with target completion by the end of next year.

It is anticipated that the advanced combustion code effort

will be completed by the end of the year 2000 providing a significant advancement in combustor design.

## Biography

Dr. Hukam Mongia graduated in 1965 from Punjab Engineering College and later received an MS and Ph.D. degrees from the University of Massachusetts. Dr. Mongia joined Garret Engine Company in 1972, where he was promoted to Senior Supervisor, Combustors, in January 1981. He, later, joined Allison Gas Turbines as Chief, Combustors R&D and CFD. He then moved to GE Aircraft engines in January of 1994, where he is employed as the Manager, Technology and Transition, combustion Center of Excellence. In this capacity, Dr. Mongia is responsible for the provision of leadership in technology, transition of technology into combustion products, and design methodology and tools. He has been involved in the design and development of numerous advanced technology and engine combustors, as well as the formulation and successful application of empirical/analytical design methodology in the combustion design process

## References

- Mongia, H. C., and Smith, K. F., "An empirical/analytical design methodology for gas turbine combustor", AIAA Paper 78-998.
- Mongia, H. C., Reynolds, R. S., and Srinivasan, R., 1986, "Multidimensional gas turbine combustion modeling: Applications and limitations", *AIAA J.*, Vol. 24, No. 6, June 1986, pp. 890-904.
- Rizk, N. K., and Mongia, H. C., 1993, "Semianalytical correlations for NO<sub>x</sub>, CO and UHC emissions", *J. Eng. Gas Turbines and Power*, July 1993, Vol. 115, pp. 603-611.
- Tonouchi, J. H., Held T. J., and Mongia, H., 1997, "A semi-analytical finite rate two-reactor model for gas turbine combustors", ASME Paper 97-GT-126
- Danis, A. M., Burrus, D. L., and Mongia, H. C., 1997, "Anchored CCD for gas turbine combustor design and data correlation", *J. Eng. Gas Turbines and Power*, 1997, Vol. 119, pp. 535-545.
- Tolpadi, A. K., Prakash, C., Hura, H., and Mongia, H. C., 1998, "Advanced combustion code: Overall description, prediction of a jet diffusion flame and combustor flowfields," ASME Paper 98-GT-
- Launder, B. E., and Sharma, B. I., 1974, "Application of the energy dissipation model of turbulence to the calculation of flow near a spinning disc," *Letters in Heat and Mass Transfer*, 1, pp. 131-138.
- Yang, Z., and Shih, T. H., 1993, "New time-scale based k-ε model for near-wall turbulence," *AIAA J.*, 31, pp. 1191-1198.
- Wilcox, D. C., 1993, "Comparison of two-equation turbulence models for boundary layers with pressure gradients," *AIAA J.*, 31, pp. 1414-1421.
- Karki, K. C., Oechsle, V. L., and Mongia, 1992, "A computational procedure for diffuser-combustor flow interaction analysis", *J. Eng. Gas Turbines and Power*, January 1992, Vol. 114, pp. 1-7.
- Nikjoo, M., and Mongia, H., 1999, "Predictions of flows with adverse pressure gradients," AIAA Paper 99-2817.
- Driver, D. M., 1991, "Reynolds shear stress measurements in a separated boundary layer," AIAA Paper 91-1787.
- Kumar, Ganesh N., Moder, Jeffrey, P., Mongia, Hukam C., and Prakash, Chander, 1998, "Development of a three dimensional radiative heat transfer computational methodology for aircraft engine combustors," AIAA Paper 98-0855
- Kumar, G. N., and Mongia, H. C., 1998, "A quasi-3D anchored radiation model for gas turbine combustors," AIAA Paper 98-3985.
- Kumar, G. N., and Mongia, H., 1999, "Validation of turbulence models for wall jet computations as applied to combustor liners," AIAA Paper 99-2250.
- Kumar, G.N., and Mongia, H., 2000, "Assessment of advanced turbulence models and unstructured code for calculating film effectiveness of a modern film-cooled combustor." Paper to be presented at the 38<sup>th</sup> AIAA Aerospace Sciences Conference, Reno, NV, January 2000.
- Sen, B., 1995, "Effects of injection hole geometry, high free stream turbulence, and surface roughness on film cooling heat transfer," Ph.D. Dissertation, University of Texas at Austin, 1995.
- Sinha, A.K., Bogard, D.G., and Crawford, M.E., 1991, "Film-Cooling Effectiveness Downstream of a Single row of Holes with Variable Density ratio," *Transactions of the ASME, Journal of Turbomachinery*, Vol. 113, June 1991, pp. 442-449
- Tolpadi, A. K., Prakash, C., Hura, H., and Mongia, H. C., 1998, "Advanced combustion code: Overall description, prediction of a jet diffusion flame and combustor flowfields," ASME Paper 98-GT-229.
- Hura, H. S., Joshi, N. D., Mongia, H. C., and Tonouchi, J., 1998, "Dry Low Emissions Premixer CCD modeling and validation," ASME Paper 98-GT-444.
- Held, T. J., and Mongia, H. C., 1998, "Application of a partially premixed laminar flamelet model to a low emissions gas turbine combustor," ASME Paper 98-GT-217
- Kim, W.-W., Menon, S., and Mongia, H. C., 1998, "Large eddy simulations of reacting flow in a dump combustor," AIAA Paper 98-2432.
- Kim, W.-W., and Menon, S., 1999, "Large-Eddy simulation of turbulent premixed flames in the thin reaction zone regime," AIAA Paper 99-2816.



As part of our efforts to improve *Naval Research Reviews*, please fill out this short questionnaire, fold in half, and return to the address printed on the back of this form.

**Organization type:**

- ☐ Government
- ☐ Non-profit
- ☐ University
- ☐ Industry

**Number of people in your organization:**

- ☐ 1-10
- ☐ 11-20
- ☐ 21-50
- ☐ 51-100
- ☐ 101-500
- ☐ 501-1000
- ☐ 1001-5000
- ☐ 5001-10,000
- ☐ more than 10,000

**Number of people in your department:**

- ☐ 1-10
- ☐ 11-20
- ☐ 21-50
- ☐ 51-100
- ☐ 101-500
- ☐ more than 500

**How many people in your department read this magazine:**

- ☐ 1-10
- ☐ 11-20
- ☐ 21-50
- ☐ 51-100
- ☐ 101-500
- ☐ more than 500

**How many people in your organization read this magazine:**

- ☐ 1-10
- ☐ 11-20
- ☐ 21-50
- ☐ 51-100
- ☐ 101-500
- ☐ more than 500

**How do you prefer to receive this magazine?**

- ☐ Hard copy
- ☐ Adobe Acrobat pdf file on CD
- ☐ Adobe Acrobat pdf file downloadable from the ONR website
- ☐ No preference

**What topics would you like to see covered in future issues of this magazine?**

---

---

---

---

---

**Any additional comments:**

---

---

---

---

---

---

---

---

**Your name and address (optional):**

---

---

---

---

---

(fold on line and tape to secure)

---

---

---

---

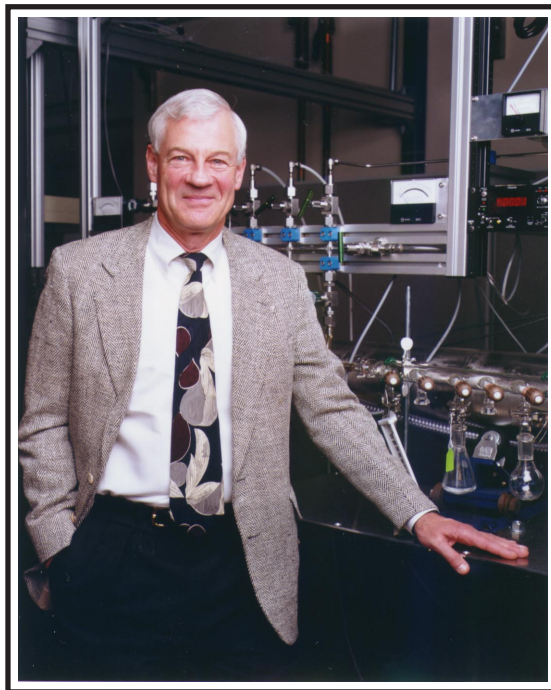
---

Post Office  
will not  
deliver  
without  
postage

**Office of Naval Research  
Corporate Communications Department  
800 N. Quincy Street  
Arlington, VA 22217-5660**

# Profiles in Science

**Professor Ronald K. Hanson**  
*Mechanical Engineering Department  
Stanford University  
Stanford, CA*



Professor Ronald K. Hanson has been affiliated with the Mechanical Engineering Department of Stanford University since 1971, where he is the Woodward Professor and Department Chairman. Professor Hanson's research has been in the fields of laser diagnostics, chemical kinetics, combustion, and propulsion. He is an internationally recognized leader in the development of laser-based diagnostic methods for combustion and propulsion.

In the 1970s he pioneered the use of tunable IR diode laser absorption spectroscopy for non-intrusive measurements of species and temperature in combustion environments. In the early 1980's his group established a method, known as Planar Laser-Induced Fluorescence (PLIF) and now used worldwide, for obtaining instantaneous 2-D images of combustion properties by means of laser excitation and digital camera recording. PLIF provides unique capability to observe complex flow structures which are currently beyond computation or measurement by other methods. Measurable quantities include species, temperature, pressure, and velocity. In the 1990s, Prof. Hanson and his students began to utilize room temperature tunable diode lasers (TDLs) as light sources in absorption diagnostics. These lasers offer high potential for rugged, compact, and economical diagnostics suitable for use in research and development. The potential of these diode lasers for sensing and control of practical combustion and propulsion systems was recently validated through a collaboration with Naval Air Warfare Center (NAWC), China Lake, CA. Prof. Hanson's group designed and implemented a multiple-wavelength diode laser system which provided rapid sensing of temperature and key species in a forced combustor at NAWC. The temperature data were used in a fast, active control scheme to optimize combustor performance, with a particular objective of achieving high combustion efficiencies and minimum emissions of pollutants such as CO and unburned hydrocarbons. This pioneering implementation was highly successful, and has led to current research on sensors for other pollutant species.

A key advance in Prof. Hanson's diode laser research was the development of measurement concepts based on the shapes and positions of absorption lines. This measurement strategy enables simultaneous determination of multiple parameters, including quantities such as mass and momentum flux, which have not been measured previously by optical means. During the past few years, under support from ONR and AFOSR, these TDL diagnostics have been applied as sensors in research on combustion control, yielding near-real-time sensing ability which has aided development of new types of forced-combustion devices of interest to the Navy. At present, Prof. Hanson's group is working to extend TDL diagnostics to control gas turbine combustors, and to new applications in advanced propulsion systems such as pulse-detonation engines.



# NAVAL RESEARCH REVIEWS

Naval Research Reviews, a theme-issue quarterly journal, publishes articles about Department of the Navy Science and Technology programs conducted by academia, government laboratories, for-profit and nonprofit organizations, and industry.

The journal is available on the World Wide Web at

<http://www.onr.navy.mil/onr/pubs.htm>



800 North Quincy Street  
Arlington, VA 22217-5660

## **Chief of Naval Research**

*RADM Paul G. Gaffney, II, USN*

## **Executive Director and Technical Director**

*Dr. Fred Saalfeld*

## **Vice Chief of Naval Research**

*BGen Timothy Donovan, USMC*

## **Director, Corporate Communications**

*Liane Young*

## **Scientific Editor**

*Gabriel Roy*

## **Managing Editor**

*Cynthia Nishikawa Fabry*

## **Technical Writers/Editors**

*Diane Banegas*

*John Petrik*

## **Design and DTP**

*Larry Behunek*

*Cynthia Nishikawa Fabry*